NTNU – Trondheim
Norwegian University of
Science and Technology

Single-Molecule Pair Studies of RGD-Coupled Alginate and Integrin

Hye Won Lee

Biotechnology (5 year)
Submission date: May 2014
Supervisor: Gudmund Skjåk-Bræk, IBT
Co-supervisor: Berit Strand, IBT
Finn Aachmann, IBT

Norwegian University of Science and Technology
Department of Biotechnology

Acknowledgments

The work described in this study was carried out as a co-project at the Department of Biotechnology with the Department of Biophysics and Medical Technology at the Norwegian University of Science and Technology.

First of all, I would like to thank my supervisors, Berit L. Strand, Bjørn Torger Stokke, Marianne Øksnes Dalheim and Finn L. Aacmann, for their support and valuable feedback on my thesis.

Secondly, I would like to thank Wenche I. Strand, Gjertrud Maurstad for great help in the laboratory.

Thirdly, I would like to thank Kristin Elisabeth Haugstad and Anna Maria Padol for helping me whenever I had troubles with JPK force robot and analysis.

Last but not least, I really appreciate my friends in Trondheim and my family in Korea who supported me during the five years of journey to accomplish my degree.

Abstract

Alginate can form a stable and non-immunogenic hydrogel with divalent ions (e.g. Ca^{2+}). Cells encapsulated in the alginate gel have high viability. Grafting alginate with RGD (Arg-Gly-Asp) peptide, an integrin binding ligand, has been shown to enhance cell attachment to the gel. In this study, AFM (Atomic Force Microscopy) was used to measure single-molecule unbinding force under nearly physiological conditions to investigate the interaction between RGD-coupled alginate and integrin.

GRGDSP(GlyArg-Gly-Asp-Ser-Pro)-coupled alginate by carbodiimide chemistry and GRGDYP(GlyArg-Gly-Asp-Tyr-Pro)-coupled periodate oxidised alginate by reductive amination resulting in 4.8% and 5.5% coupling efficiency, respectively, were tested for interaction with $\alpha_5\beta_1$ integrin. Alginate was immobilised on the AFM cantilever by carbodiimide chemistry or by reductive amination, while integrins and other proteins were immobilised on a silica surface by carbodiimide chemistry. Integrins were either randomly immobilised or captured by antibody CD 29. Despite variation of the alginate on the tip and of the immobilisation method for both alginate and integrin, specific interaction was not possible to measure. Antibody surface and insulin surface were tested as non-interactive surfaces with RGD-coupled alginate, however the same level of interaction was found for these surfaces as for the integrin surfaces. Silane surface was not supposed to show any interaction, but it showed stronger interaction with RGD-coupled alginate than when proteins were immobilised. Furthermore, blocking of the interaction by the addition of soluble RGD peptide did not show any effect on reducing the interaction frequencies.

The overall conclusion from this study is that no specific interactions could be measured between RGD-coupled alginate and $\alpha_5\beta_1$ integrins. This work aims to assist future investigations regarding the same system.

Table of Contents

List of Figures

List of Tables

Nomenclature

M	β-D-mannuronic acid
G	α-L-guluronic acid
RGD	Arginine-Glycine-Aspartic acid
GRGDSP	Glycine-Arginine-Glycine-Aspartic acid -Serine-Proline
GRGDYP	Glycine-Arginine-Glycine-Aspartic acid-Tyrosine-Proline
POA	Periodate Oxidised Alginate
Alg-GRGDSP	GRGDSP-coupled alginate
POA-GRGDYP	GRGDYP-coupled periodate oxidised alginate
AFM	Atomic Force Microscopy
OT	Optical Tweezers
MT	Magnetic Tweezers
DFS	Dynamic Force Spectroscopy
DoF	Degree of Freedom
EDAC	l-ethyl-3-(3-dimethylaminopropyl)carbodiimide
HEPES	4-(2-Hydroxyethyl)piperazine-1-ethanesulfonic acid
TETA,	N-(Trimethoxysilylpropyl) ethylenediamine triacetic acid, trisodium salt
TDET	N^1-(3-Trimethoxysilylpropyl)diethylenetriamine
MQ	Milli-Q
NMR	Nuclear Magnetic Resonance
ITC	Isothermal Titration Calorimetery
QPD	Quadruple Photodiodied
PHSRN	Proline-Histidine-Serine-Arginine-Asparagine
SLB	Supported Lipid Bilayer
DP	Degree of Polymerisation

1 Background

Biomaterials have evolved since the late 1960s with the development in biology and materials science [1]. The main research focus has been the chemical and biological inertness of the materials for implantation [2]. However with the progress of understandings in molecular biology, attention has shifted towards the need for specific and direct interactions between the biomaterials and the tissue components [1, 2]. Applications of such biomaterials enables sophisticated control systems in tissue engineering, drug and gene transfection delivery systems, medical nano- and biotechnologies as well as implantable medical devices [2].

In the field of tissue engineering and regenerative medicine, hydrogel scaffolds are of particular interest due to their innate biocompatibility and flexibility towards modification. There has been increasing importance for biomaterials such as proteins (collagen, elastin and silk) and polysaccharides (hyaluronan, alginate and chitosan) as they can achieve two critical functions as scaffolds: shape determination of regenerative tissues and facilitation of the appropriate cell behaviour [2]. Alginate has given special interest as it can form a very stable and non-immunogenic hydrogel with divalent ions such as Ca^{2+}. In addition the alginate matrix provides an environment for cells to keep high viability when cells are seeded [3].

In many cell types, the integrin mediated cell attachment influences cell migration, growth, differentiation and apoptosis [4]. Therefore, the application of the integrin-binding-peptide (RGD) coupled alginates for tissue engineering has been recognised and investigated. In spite of the advantageous features of peptide coupling to alginate, the system has not been fully investigated.

The purpose of this study is to obtain the physical binding strength between a single integrin and integrin-binding-peptide coupled on alginates. Comparing the values of single molecular interactions measured from the same interaction occurring in the biologically driven materials will give insight to the degree of bio-mimicity and efficiency of the peptide coupled alginate scaffold.

2 Aim

Characterising the single molecular pair interactions between purified $\alpha_5\beta_1$ integrins and RGD coupled alginate with atomic force microscopy (AFM) will provide insight into the efficiency of the RGD-coupled alginate in cell capturing in single molecular scale. The result could be compared with existing interaction profiles between the integrins and fibronectins, which are part of the natural extra cellular matrix (ECM) that contains RGD sequence. The adhesion/de-adhesion mechanisms of RGD coupled alginate could be used to determine its critical influence on the cell migration, growth and development of stem cells.

As the interactions were not successfully measured due to the obstacles defined in this thesis and time constrains, this thesis is written in order to assist the future investigation regarding the same topic.

3 Introduction

3.1 Alginates properties and applications

Alginate is a family of polysaccharides that is extracted from marine brown algae for commercial use [5]. Its main function in algae is to provide the plant mechanical strength and flexibility, and it consists up to 40% of the plants dry matter [6]. Its unique temperature independent characteristics, such as cold solubility and cold setting gels, have resulted in alginates being used as a popular food additives [7]. Alginates are also synthesised by two bacteria genera, *Azotobacter* and *Psudomonas*, as a form of exopolymeric polysaccharide [8].

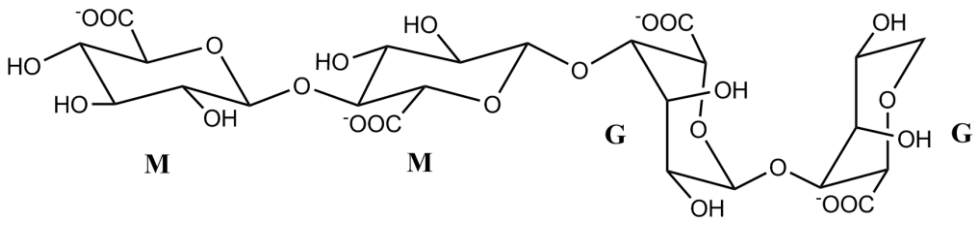

Figure 3.1. Structure of alginate
M, (1→4)-linked β-D-mannuronic acid, and its C-5 epimer, G, α-L-guluronic acid. Reproduced from Draget (1997) [9].

3.1.1 Chemical properties

Alginates comprise an unbranched block copolymer composed of units of (1→4)-linked β-D-mannuronic acid (M) and its C-5 epimer α-L-guluronic acid (G) (Figure **3.1**). Homopolymeric domain of mannuronan (··MMM··) is called M-blocks, that of guluronan (··GGG··) is called G-blocks and heteropolymer (··MGM··) domain is called MG-blocks. Epimerase enzymes convert M-block which is the initial form of alginates into the C-5-epimer guluronan, producing three types of blocks; G blocks, MG blocks and the remaining M blocks. Seven natural epimerases (AlgE1 ~ AlgE7) have been identified in *Azotobacter vinelandiiand* of its mutants with improved functionalities to generate G-rich alginates have been produced [10, 11]. With the

advent of gene technology, it is becoming popular to tailor design alginates with desirable distribution of M and G blocks [12].

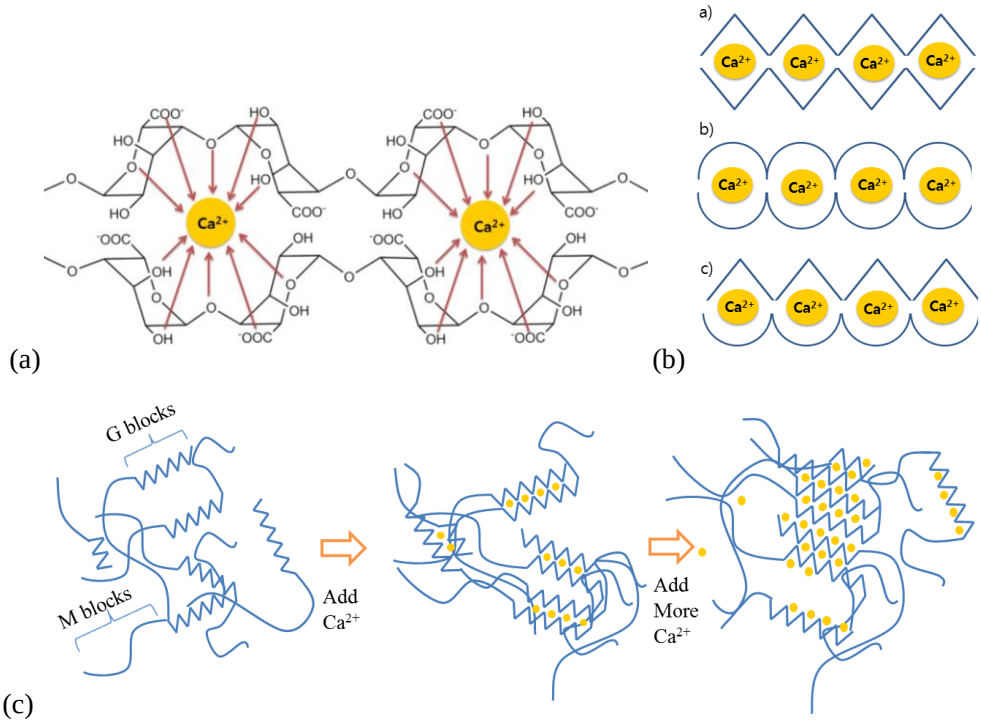

Figure 3.2. Gelation of alginate hydrogel

(a) Binding site formation with four consecutive G-residues. reproduced from [13]. (b) 'egg in box' models with a) G-blocks b) MG alternating block c) MG alternating block and G-block, reproduced from [14]. (c) Formation of G blocks chains and lateral association.

3.1.2 Gelation

G block distribution is critical in alginate gelation. Smidsrød (1970) shown that G blocks selectively bind to divalent ions and form gels or precipitate (Figure 3.2 (a)) in the following strength; $Ba^{2+} > Sr^{2+} > Ca^{2+} > Mg^{2+}$ [6]. In addition with increasing fractional Ca^{2+} saturation of guluronic acid, higher lateral polymer association of chain segments were observed [15] (Figure 3.2 (c)). As shown at Figure 3.2 (b), alginates with MG alternating sequence share the similar gelation property with the G blocks upon treatment with calcium ions [14].

Such gelation property with calcium is beneficial as the process doesn't require any toxic crosslinking agent, and toughness and stiffness of the gel can be controlled by the concentration of divalent ion added.

3.1.3 Alginate as biomaterial

Alginates are very promising biomaterials for entrapment and delivery of cells and proteins [16]. First, the alginate hydrogels can be highly hydrated achieving up to 99% of aqueous media contents. Such high porosity enables effective incorporation of biological cue molecules in the media as well as effective exchange of nutrients and removal of wastes through the gel. Alginates gels are highly hydrophilic, so that the alginate give low protein absorption and low immunogenicity *in vivo* [16, 17]. In addition, alginate is degraded *in vivo* via a process involving loss of divalent ions to the surrounding medium and subsequent hydrolysis. This makes alginate a very popular material for tissue engineering [18].

One of the very common forms of alginate use is macro/microencapsulation [19]. It was achieved by dropping cell-suspending alginates into a calcium or barium solution. Dufrane et al. (2006) have demonstrated up to 6 months survival of encapsulated pig islets of Langerhans, while non-encapsulated islets were rapidly destroyed in primates [20]. In order to increase the stability and efficiency of targeted delivery, alginate microspheres have been tailored using advanced techniques and the following alginate microspheres are currently available; layer by layer assembled alginate beads, muco-adhesive, polymer-coated, site specific targeted, magnetic, bioactive-ceramic, silicate, hyaluronic acid or thermo and pH responsive alginate microspheres [21].

Alginate hydrogel can be injected into damaged tissue and assist cell therapy and tissue regeneration. This procedure is minimally invasive, facilitate the incorporation of therapeutic agents and cells, efficient at filling irregular defect sites due to high contourability [22]. Thus alginate gel has potential applications to replace current multiple surgeries [23].

3.1.4 Limitations

Independently of advantages and efficacies, the hydrophilic nature of alginate results in low protein adsorption, and cells are unable to interact with the alginates via cell surface receptors or ligand [24]. Alginate derivatives have been introduced in order to alter physiochemical and biological properties such as solubility, hydrophobicity, cell

receptor binding etc. In this study, the interaction properties between integrin-ligand, RGD, bound alginates and its receptors (integrins) will be studied.

3.2 Cell binding proteins, integrin and RGD

3.2.1 Integrin

Integrins are heterodimer receptor molecules with the main function in mediating cell adhesion and communication between the extracellular and intracellular environments of the cells [25, 26]. For approximately 30 years ago, integrins have become the most studied receptor molecule, as their importance in immune response, cancer development, haemostasis and a series of other functions has been identified [27]. So far, 18 α-units and 8 β-units have recognised, and 24 different non-covalently associated receptor combinations have been identified (Figure 3.3) [28]. Among them, five combinations are known to have RGD as its ligands. This study has focused on human integrins $\alpha_5\beta_1$. They are one of the most investigated receptors that shows specificity for the RGD sequence, and they are found in several cell types: fibroblasts, platelets, monocytes and lymphocytes [29].

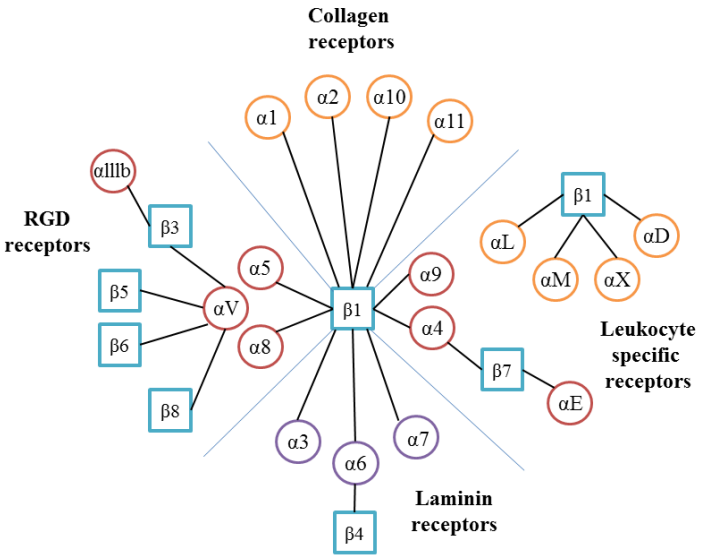

Figure 3.3. Integrin family

24 heterodimer combinations are found in vertebrates. Reproduced from Barczyk (2010) [28]

Integrins are transmembrane protein that consist of three parts: an ectodomain, a memebran spanning domain and an endodomain. In more detail, Figure 3.4 represents the $\alpha_5\beta_1$ integrin with the divalent ion binding sites indicated.

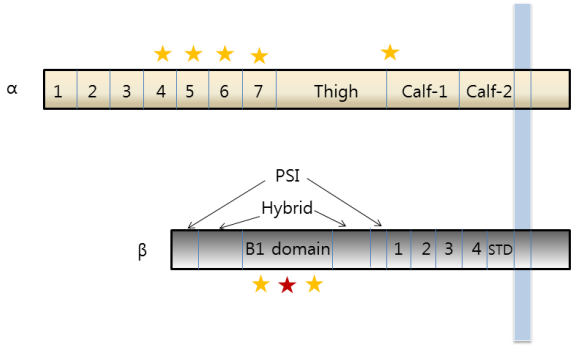

Figure 3.4. Representation of prototypical $\alpha_5\beta_1$ domain integrin heterodimer
Yellow stars indicate calcium ion binding sites and the red star indicates a metal-ion-dependent adhesive site.

3.2.2 RGD

RGD is a ligand for integrins and it is found as part of the ECM (Extra Cellular Matrix). The ECM mainly consists of glycoproteins and proteoglycans, such as fibronectin and collagen. It entraps and transmits signal molecules among vicinal cells, and such cues contained in ECM determines cell migration. It is the major component of animal tissue, filling up the space between cells. It provides supports and cell-anchoring sites by exposing specific ligand for receptors of cells. The most investigated cellular recognition sequence in ECM is RGD.

Interaction between $\alpha_5\beta_1$ and RGD is well known to have a critical function in vertebrate cell development. For example, deficiency of $\alpha_5\beta_1$ resulted in failed embryonic angiogenesis in mice [30], and P.Pimton et al. (2011) have found that fibronectin and $\alpha_5\beta_1$ integrin are influential to the meso-endodermal differentiation of mice embryonic stem cells [31].

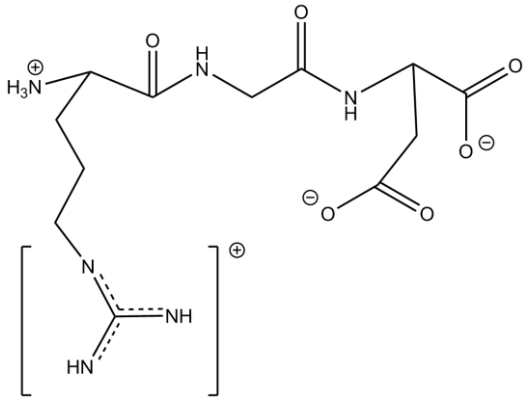

Figure 3.5. Tripeptide Arginine-Glycine-Aspartate (RGD) in physiological pH

RGD peptides and its analogues have been grafted to various biomaterials in order to enhance cell viability and to control cells and stem cells differentiation, or have been synthesised in the solubilised form as cell-adhesion inhibitor [32]. GRGDSP is the sequence found in fibronectin, and has been thoroughly incorporated in biomaterials. Many different RGD-containing peptide sequences have been also tested and found to have affinity to $\alpha_5\beta_1$.

3.2.3 Integrins bind RGD

RGD is known to bind at the top of the head domain of $\alpha_5\beta_1$ [33]. The most classical RGD-containing ECM protein is the type III fibronectin domain; it binds to integrins as described in Figure 3.6. Ligand recognition of integrin is unique in three aspects. Firstly, the ligand is determined combinatorially by two hetero dimers. Although $\alpha_5\beta_1$ and $\alpha_v\beta_1$ share the same β_1 subunit, $\alpha_5\beta_1$ takes fibronectin as a ligand while $\alpha_v\beta_1$ takes vitronectin as well as fibrinogen as ligands [34]. Secondly, integrins contain metal ion-dependent adhesion sites and the divalent metals bound in these sites associate with the carboxylic group in the ligand, stabilising the bond. Lastly, the binding activity requires conformational changes [33].

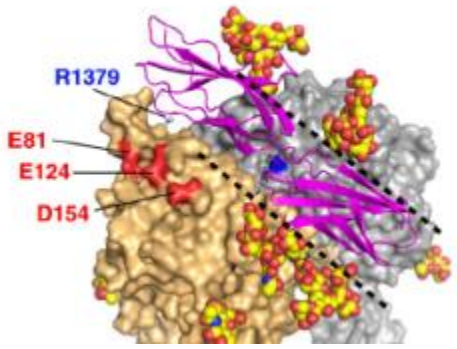

Figure 3.6. A model of fibronectin Fn9-10 docked onto the $\alpha_5\beta_1$
α_5 (wheat colour) and β_1 (grey colour) are in space filling model. RGD is shown as green stick model within the fibronectin (magenta ribbon model) taken from protein data bank accession no. 2MFN. Blue head surfaces are a metal-ion-dependent adhesive site. Taken from M.Nagae (2012) [33].

3.2.4 Activation of integrin binding

Without any stimulation, $\alpha_5\beta_1$ usually stay in a bent conformation and show very low activity [35, 36]. It is widely accepted that with the help of divalent ions and presence of peptide ligands, integrins transform into the upright conformation readily able to catch the ligand present (Figure 3.7). The effect of divalent ions on the affinity of $\alpha_5\beta_1$ to ligands was measured as early as 1995, showing that Mn^{2+} and Mg^{2+} promoted high levels of binding whereas Ca^{2+} showed inhibitory function [37]. Such effect of ions is explained by S.Tiwari's experiment (2012): Ca^{2+} helps to stabilise the inactive bent formation of integrin during the production and intracellular transportation of integrin, where Ca^{2+} concentration is naturally high. As the integrins arrive the cell surface, Mn^{2+} or Mg^{2+} substitute Ca^{2+}, changing integrins to the active conformation [38].

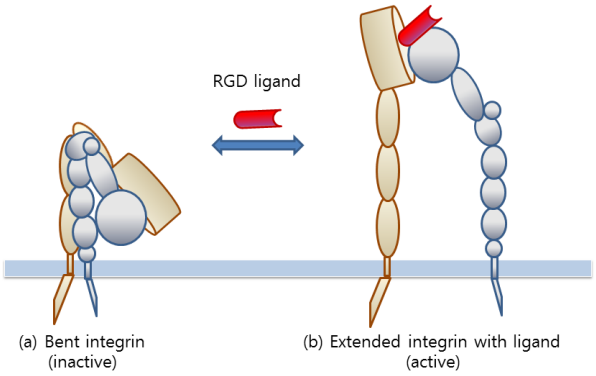

Figure 3.7. Representation of integrin arrangement and its conformation change under the presence of ligand
Reproduced from J.Takagi and T.Springer (2002) [39].

3.3 Grafting peptides to alginates

Binding activity of RGD to integrins has been reproduced by synthetic RGD containing sequences, which has been widely used on experiments to stimulate cell adhesion [4]. GRGDSP has been the most used linear sequence, while other amino acids have been introduced before and after the RGD sequence to provide extra flexibility and control functionality. It was shown by Beer et al (1992), that increasing numbers of Glysines between the polymer and the grafted RGD sequence (up to 19 Glysines) resulted a higher number of platelet binding [40].

In this study, grafting of an RGD-containing peptide sequence on alginate has been introduced with two different coupling mechanisms: 1) carbodiimide reaction on intact alginate and 2) reductive amination to periodate oxidised alginate.

3.3.1 Carbodiimide reaction

Carbodiimide coupling of peptide to alginate was first patented in 1998 [41]. It utilises the carbodiimide enzyme family, such as EDAC (l-ethyl-3-(3-dimethylaminopropyl) carbodiimide) in order to produce an amide bond by conjugating the carboxylic group on alginate chain with the terminal amine groups on the peptides. As Figure 3.8 shows,

the carboxylic group on alginate is attacked by EDAC, it forms an intermediate complex, and it is replaced by a peptide, in this case GRGDSP.

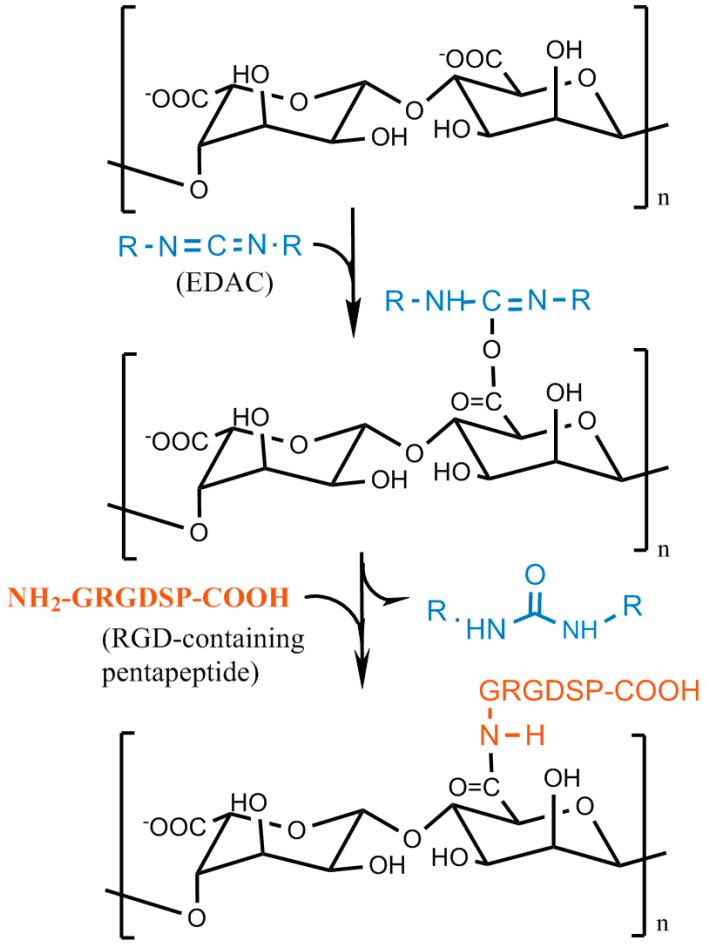

Figure 3.8. Carbodiimide reaction for coupling of GRGDSP on alginate
Reproduced from K.Bouhadir et al. (1998) [41].

Possible side reaction can be speculated since arginine (R) contains two amine groups on its side chain that can react with a carboxylic acid. As the ligand is partially immobilised on the backbone chain, the affinity of RGD to integrins will significantly be reduced. However, arginine is slightly protonated during the reaction in weak acidic

conditions so that the N-terminal of the amino acid is more readily available for the reaction by EDAC.

Grafting RGD containing peptide by the carbodiimide reaction is relatively simple as it is one-pot reaction in aqueous condition without the use of any toxic chemicals. However it achieves only 0.1 ~ 0.4 % of grafting of carboxylic group in the alginate [42].

3.3.2 Periodate oxidation and reductive amination coupling reaction

Partial oxidation of alginate was implemented in order to increase reactivity and flexibility of alginates while maintaining their ability to crosslink with divalent ions. [43, 44]. As Figure 3.9 shows, sodium periodate oxidises the bond between C-2 and C-3 in the sugar monomer, resulting in two free aldehyde groups [45]. Such oxidation is random and occurs in the equimolecular ratio up to 50% [43, 46]. Aldehyde groups are used as intermolecular crosslinking sites or amination sites.

Reductive amination connects the amino groups of the coupling molecule to the reducing end of carbonyl group (either aldehyde or ketone), forming a Schiff base covalent bond and then the conjugated groups are stabilised by reducing the bond to a secondary amine by reducing agent. 2-picoline borane is a reducing agent for reductive amination, and has been used due to its nontoxicity compared to the traditional reducing agent, sodium cyanoborohydride that produces toxic hydrogen cyanide [47]. It has been shown that only limited percentage of the free aldehyde groups are reactive [43]. In the studies from K.Kristiansen et al (2009), only half of the available aldehyde groups are coupled, even though excess amount of labelling molecules was introduced, [48].

POAs are more susceptible to acid hydrolysis in mild acidic condition than intact alginate [49, 50].This is advantageous for many tissue-engineering applications, where degradation of the matrix over limited time is wanted. Without a high degradation rate, high molecular alginate chains can accumulate and became toxic, as they cannot be excreted by urine [51]. Moreover, the degradation of alginate can be controlled by changing its degree of oxidation [52].

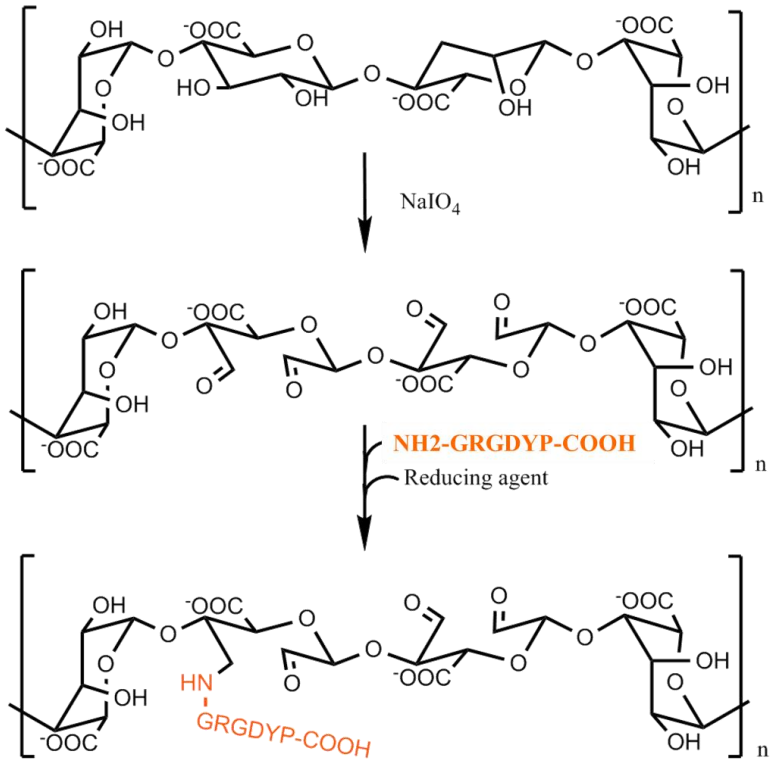

Figure 3.9. Periodate oxidation and reductive amination to couple GRGDYP on POA
Reproduced from K.Bouhadira et al. (1999) [45].

However periodate oxidation greatly increases the flexibility of the alginate chain and reduces the molecular weight (chain length), significantly eliminating the gelling properties of alginate due to changes in the distribution of G blocks and increased local chain flexibility [49]. It has been shown that gelation cannot be achieved for an alginate with over 10 % periodate oxidation [43].

3.4 Dynamic force spectroscopy

3.4.1 Significance of single molecular interactions

With the advance of measurement technologies, single-molecular spectroscopy emerged as a very attractive methodology to study the dynamics of molecular interactions. It is a powerful tool to investigate the interaction dynamics, which can be often masked by ensemble measurement. Knowledge about single molecular interactions will provide a better understanding of the interactions and it could be of benefit for designing nano-scale materials optimised for the molecules of interest.

Biological molecules form weak non-covalent bonds with each other in order to form complex structures, move, and adhere. Unlike covalent bonds, which are very stable, the interactions between ligand and receptor molecules are very weak and have limited lifetime, as they dissociate spontaneously. If a pulling force is applied to the molecules for a particular length of the time, the bond will rupture. The unbinding force of such system has been a subject of interest.

3.4.2 Dynamic force spectroscopy and Atomic force microscopy

Dynamic force spectroscopy is a technique that was developed to measure single molecular force interactions, e.g. bond strengths and bond lifetimes. Ultra-sensitive probes are used to control the pulling strength down to pico-newton scales. Atomic force microscopy (AFM), optical tweezers (OTs) and magnetic tweezers (MTs) are the main instruments used to measure single molecular interactions. As

Table **1** shows, different instruments are used depending on the system of investigation. Each instrument uses different detection techniques for the measurement of force, but the principle is the same. First, the molecules or cells of interests are sparsely immobilised on a surface or a probe. The second step is to bring the molecules close enough so that a non-covalent bond is formed between the two molecules. The last step is to separate the bond with either constant speed or constant force. The forces at which the bond ruptures are measured. Thousands of measurements of single molecular rupture forces are recorded in order to find the most likely force. In addition, the values are obtained within different order of magnitudes of loading rate, so that the trend of the rupture values influenced by different condition is obtained. By extrapolating the

trend to zero force, the physiological (where no external force is applied) interpretation of the bond is possible.

Table 1. Diverse Single Molecular Spectrometry

Spectrometry	Force range (pN)	Features	Limitation
Optical tweezers	0.1 - 100	3D manipulation	High sensitivity Photodamage Local heating
Magnetic tweezers	0.001 – 100	Sample rotation 3D manipulation	Little experiment data available Slow feedback
AFM	10 - 1000	Much experimental data available Accessible	Cantilever calibration Lacks specificity and exclusivity

3.4.3 Atomic Force Microscopy

Since the invention of atomic force microscopy for imaging in Å ngstrom resolution in 1986, AFM has developed not only as an imaging tool, but also as an instrument to measure interaction force with great sensitivity [53].

AFM consists of a piezoelectric stand, a cantilever, a cantilever holder, a laser source, a quadrant photodiode (QPD), and a computer governing the feedback system. The tip of cantilever and the surface on the piezoelectric stand are immobilised with the molecules of interest.

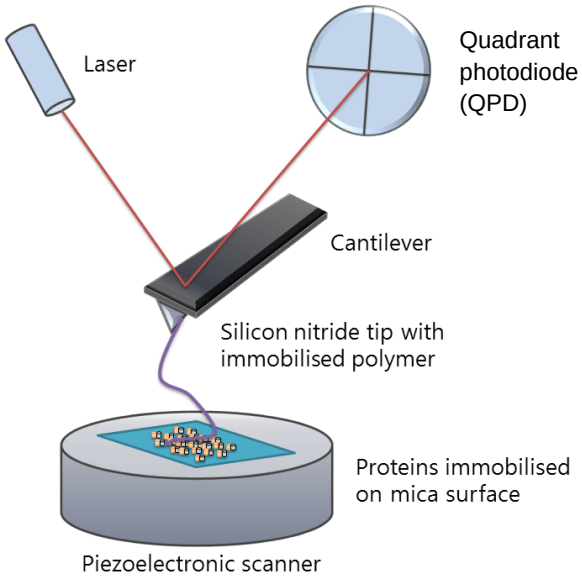

Figure 3.10. Schematic illustration of an atomic force microscopy
Immobilised polymer and proteins are also represented. Reproduced from M.Sletmoen et al. (2009) [54]

As the tip moves up and down with defined speed and distance near the surface, non-covalent bonds are formed and ruptured between the molecules. The flexible cantilever act as a spring and it is deflected according to the force exerted to cause a bond rupture. The laser beam is reflected at the top of the cantilever and reaches at the QPD. The larger the deflection of the cantilever, the farther away the laser is displaced from the centre of QPD. If the spring constant of the cantilever is known from previous calibration, the degree of displacement is converted into force. If necessary, the piezoelectric stand moves up and down as a feedback reaction in order to control the constant force exerted on the bond. A typical bond rupture profile follows Figure 3.11.

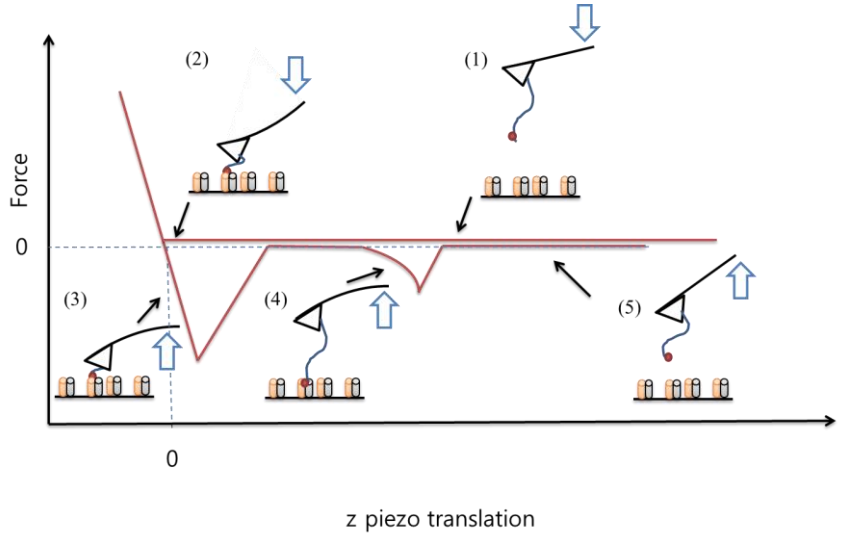

Figure 3.11. Force-extension curve obtained for a protein-polymer interaction
(1) The tip approach the surface. (2) The tip reach the surface, non-covalent bond between the ligand and the receptor is formed during the extended delay time. (3) The tip is lifted and the cantilever deflects as the surface and tip Van der Waals force drags the tip. As such tip to surface non-specific interaction is strong, the first deadhesion gives a large peak at the first detachment. (4) The more force is exerted to the tip and the polymer is straightened while the ligand and the receptor bond is still intact. (5) Finally, rupture of the non-covalent bond is observed and corresponding deflection of the tip is indicated as a small peak. Reproduced from Gomez-Casado et al. (2013) [55].

3.4.4 Calibration

Cantilevers micro-fabricated by microlithography techniques were developed as a response to the need for cantilever with low force constant (i.e. higher flexibility) and higher resonance frequency [56]. Commercially mass produced cantilevers achieve high lateral uniformity, however the precise control of the thickness is difficult. The spring constant is strongly dependent on the thickness of the cantilever, and it has been an issue that the thickness of cantilevers could deviate up to 25% of an intended value [57]. Therefore, calibration of the cantilever is essential [58]. Under the immobilisation process of the tip, the mass and the geometry of the tip can be changed with acidic chemicals, and the tips can be subjected to temperature changes by chemical reactions. Therefore, in dynamic force spectroscopy calibration of the tip is essential in order to obtain a reliable magnitude of interaction forces. Unfortunately the uncertainty in the

spring constant calibration in the cantilever is lies between 10 to 30%, according to A.Slattery et al. [59].

P.Cumpson et al. (2008) classified calibration methods into three categories: the theoretical method, the dynamic method and the thermal method [58]. The theoretical method can result in a large error, while the dynamic method has a risk of destroying the tips. J.L.Hutter and J.Bechhoefer have suggested non-destructive procedure for calibrating individual cantilevers and tips by measurement of thermal fluctuations in 1993 [60]. This method uses the equipartition theorem to relate the thermal noise of a cantilever in a liquid medium to its spring constant [61].

3.5 Theory of Single Molecular unbinding

3.5.1 Free energy landscape

The free energy landscape is a map of free energy of all the possible conformation possessed by a molecule or a molecular complex. The more complex the molecular system is the more rugged the energy landscape becomes, as it depends on the degree of freedom (DoF) the molecule has. The DoF is determined by factors such as monomer dihedral rotation, backbone bond vibration and electronic states or transition, vibration and rotation of the molecule.

Energy landscape can be depicted in a 3D contour graph but for simplicity it is often shown in a 1D line (Figure 3.12) In a non-covalently bound molecular system, the Gibbs free energy reach its lowest point (Figure 3.12 pointed with an arrow) as the system is stably bound and it seeks for the most energetically efficient conformation. When the bond dissociates, it chooses one of the numerous energy pathway for unbinding as it diffuses along the surface of the energy landscape [62]. In biological systems, a large number of molecules are involved in the energy system, thus several semi-stable conformations can be identified, where the system is relatively stable and can have long lifetime.

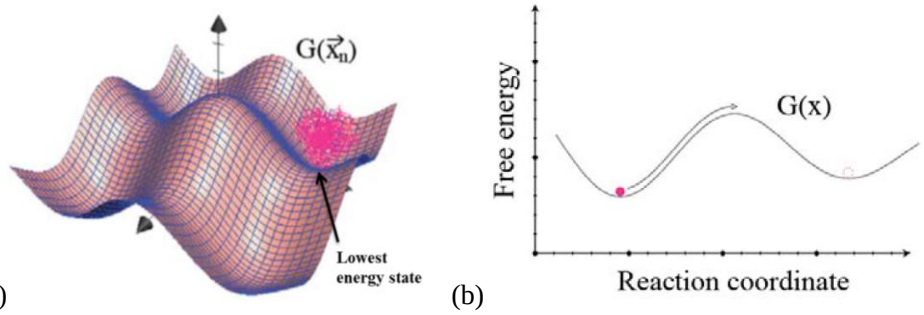

Figure 3.12. Energy landscape of receptor and ligand binding

(a) 3D representation of a free energy landscape $G(\vec{x}_n)$ with an arbitrary system. (b) A free energy landscape $G(x)$ of a particle in 1D free energy surface. Taken from A.Håti (2012) [63].

As the system can be highly complicated, it was attempted to simplify the system by dividing the energy profile into several pieces containing only one transition state. This is called a two states approximation [62] .

3.5.2 Force application and statistical analysis

The previously shown free energy landscape becomes distorted if a force is applied. Evans and Ritchie (1997) outlined a theory of the kinetics of bond dissociation under the influence of force [64].

$E_b(x)$ is the energy barrier at the transition state without any external force applied. When force f is applied to the system along the reaction coordinate x, the energy landscape is tilted.

$$E_b(f,) = E_b - f x_\beta \tag{3.1}$$

$$x_\beta = < x_{ts} \cos\theta > \tag{3.2}$$

where, x_β is the thermally averaged projection (Figure 3.13).

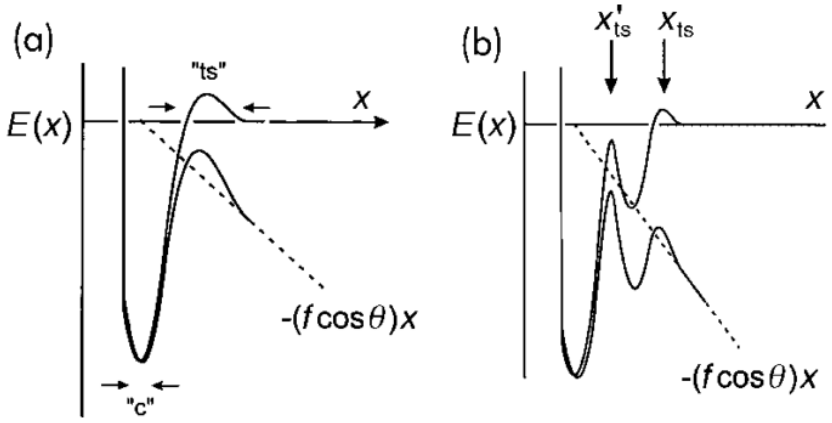

Figure 3.13. 1D energy landscape
For bound state "c" and activation barrier (peaks). External force f added that tilts the energy landscape and lowers the barrier. Images are taken from E.Evans (1998) [65].

As the energy barrier is lowered by the force applied, the rate of escape can also be reduced. Such model is represented by the following equation

$$k_{off} = \frac{D}{l_c l_{ts}} exp\left[\frac{-E_b(f)}{k_B T}\right] \tag{3.3}$$

where, k_{off} is the rate of dissociation events, k_B is the thermal energy and $\frac{D}{l_c l_{ts}}$ is the attempt frequency, D is the diffusion constant, l_c is the confinement of the bound state and defines the entropy gradient which drives the escape and l_{ts} is the local barrier of the transition state [66].

This analysis of the tilted energy landscape gives extra insight about the interaction. The added energy by applied force acts more strongly on the outmost energy barrier by tilting it a greater degree compared to the inner barrier. Thus, the inner barrier, which is usually masked by the outmost barrier, can be exposed and can be studied.

The rupture force is highly dependent on the loading rate.

$$r_f = kv \equiv \frac{df}{dt} \tag{3.4}$$

where r_f is the loading rate, k is the spring constant and v is the separation speed. A large loading rate gives a high rupture force (f) and short dissociation time (t), and vice versa. When the loading rate is very small, and the dissociation time becomes longer than a finite lifetime of the non-covalent bond, the spontaneous unbinding due to the fluctuation of surrounding, rather than the force applied, will happen. This value may be the focus of interest when studying bond ruptures within a physiological state.

The probability density function can be applied for a single bond unbinding event, as it is a stochastic event.

$$\mathrm{P}(f) = k^0 exp\left(\frac{x_\beta f}{k_B T}\right) exp\left[\frac{k^0 k_B T}{x_\beta r_f}\left(1 - exp\left(\frac{x_\beta f}{k_B T}\right)\right)\right] \tag{3.5}$$

Where k^0 is the dissociation rate before force is applied.

This formula was fitted to the histograms made from repeated observations of single molecular rupture under the small range of loading rate as shown in Figure 3.14.

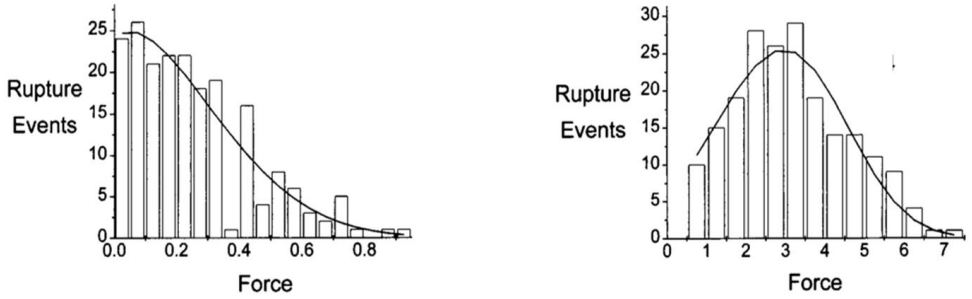

Figure 3.14. Examples of curve fitting to the force histogram
The distribution is measured from simulation of single molecular interaction bond Image is taken from E.Evans and K.Ritchie (1997) [64].

At each one of the specific loading rate ranges, the most likely rupture force is found by the probability density function. The rupture force is plotted against the log value of the loading rate: this is called a dynamic force spectra. A single barrier interaction will give a positive linear graph with one slope. If there were more than one barrier involved, a change in the slope of the line would be found. Since the inner barrier is less tilted by the external force applied, the slope gets steeper.

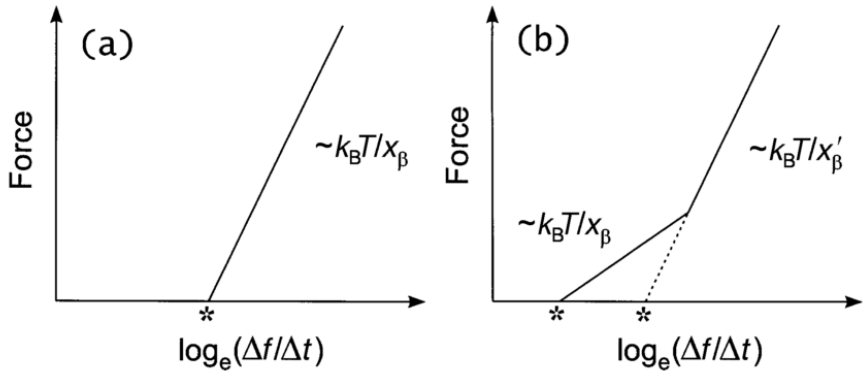

Figure 3.15. Dynamic force spectra for unbinding

Over one activation barrier (a) and two activation barriers (b) Image is taken from E.Evans (1998) [65].

4 Materials and Methods

4.1 Alginate

4.1.1 Alginate-GRGDSP by carbodiimide reaction

GRGDSP coupled with a high G-content, high MW alginate was purchased from FMC Biopolymer. Analysis sheet and calculation for the degree of peptide coupling is included in Appendix A.

4.1.2 Reductive amination for GRGDYP coupling on POA

Two batches of POA were used for further peptide coupling. The first batch was 8% periodate oxidised alginate (LF10/60, Mw = 103300g/mol) provided by Marianne Ø ksnes Dalheim (PhD. Candidate at the Department of Biotechnology, NTNU). For the second batch, alginate with higher molecular weight (HF 120RB, Mw = 271000g/mol, F_G = 0.48) was used in order to increase the average chain length of alginate and periodate oxidation was carried out with assistance of Marianne Ø ksnes Dalheim.

Periodate oxidation was a one-pot reaction. The alginate was dissolved in 10% n-propanol aqueous solution (3.0mg/ml). In order to reduce free radical formation from oxygen, all the solutions were nitrogen gassed. As the sodium periodate is sensitive to light, all the reactions were carried out in a dark environment. Equimolar amounts of IO_4Na to the degree of oxidation desired were added to the mixture. The reaction ran for 48 hours at 4˚C.

For RGD coupling, an alginate solution (3.0mg/ml) in MQ-water and methanol (12% (v/v) for the final solution) was made. 50mM GRGDYP (Caslo Laboratory) was added to the alginate solution, twice higher molar concentration than the concentration of oxidised monomers. 0.25M 2-picoline borane complex (95%, Sigma-Aldrich) in methanol was used in 20 times higher molar concentration of the number of aldehyde groups available in POA. 2-picoline borane is a non-toxic reducing reagent that connect aldehyde groups in alginate to amine groups in silane by the formation of a Schiff base covalent bond and reduction of the nitrogen to a secondary amine [47]. The reaction was carried out for 48 hours at room temperature and dialysed (MWCO 12-

14000, Spectro/Por) in two steps: firstly against two shifts of 0.05M NaCl to remove excess peptide and 2-picoline borane, and secondly against MQ-water until conductivity was less than 0.2μS in order to remove the salts. After dialysis, the solution was freeze dried for storage.

4.2 Immobilisation of alginate and integrins

Recombinant human integrin $\alpha_5\beta_1$ (R&D systems), bovine insulin (Sigma-Aldrich), anti-human CD29 (β_1) antibody (Biolegend) were used.

Either GRGDSP-coupled alginate (Alg-GRGDSP) or GRGDYP-coupled POA (POA-GRGDYP) were covalently immobilised on silicon nitride AFM tips. On the mica surface, either integrin captured by antibody, antibody, silane or antibody was immobilised.

AFM tips and freshly cleaved mica surfaces were cleaned in a methanol and HCl (1:1 v/v) solution. This step ensures that the surface evenly exposes the hydroxyl groups that will further react with silanes. The tip was incubated in (1% or 3% (v/v)) silane, TDET (N^1-(3-Trimethoxysilylpropyl)diethylenetriamine) in (1mM) acetic acid for either 10 minutes or 30 minutes. The mica surface was coated with (1%, 2% or 5% (v/v)) TETA, (N-(Trimethoxysilylpropyl) ethylenediamine triacetic acid, trisodium salt; 45%) in (1mM) acetic acid for either 10 minutes for 25 minutes. Exact concentration used was indicated on Table 2.

Two different methods were used for covalent immobilisation of RGD coupled alginate on the silicon nitride tip. For the carbodiimide immobilisation reaction, the silanised tips were immersed in 0.5 to 1.0mg/ml of alginate solution in (5mM) boric acid in pH 5.8. EDAC, (N-(3-Dimethylaminopropyl)-N´-ethylcarbodiimide Hydrochloride, Sigma-Aldrich), was weighed 10% by mass of substrate and added to the solution. EDAC is a catalyst that attacks carboxylic groups of alginate and form a covalent bond with the amine groups of the end of the silanes on the tip. As the effectiveness of EDAC lasts only for 0.5 to 1 hour, EDAC was added right before the reaction.

For the reductive amination immobilisation method, silanised tips were immersed in an alginate solution (0.5 to 1.0 mg/ml) in MQ-water and Methanol (12% (v/v) for the final solution). 0.25M 2-picoline borane in methanol (4% (v/v) for the final solution) was

added. The reaction was incubated from 4 hours to 8 hours depending on the wanted density of the alginate on the tip.

Surface immobilisation on silanised mica surface was preceded by the carbodiimide reaction for all of the substrates. Integrin (50μg/ml), insulin (100μg/ml) and antibody CD29 (250μg/ml) solutions were made in 5mM boric acid with pH 5.8 with EDAC (10% by mass of the substrate). In order to capture the integrins with the antibodies, integrin (100μg/ml) was added to the surface-immobilised antibody after 30 minutes of reaction.

Incubation times for alginate immobilisation were varied between 30 minutes to 2 hours in order to control the number of alginate molecules bound to the tip. For surface immobilisation, more than 2 hours were used. All of the reactions proceeded at room temperature.

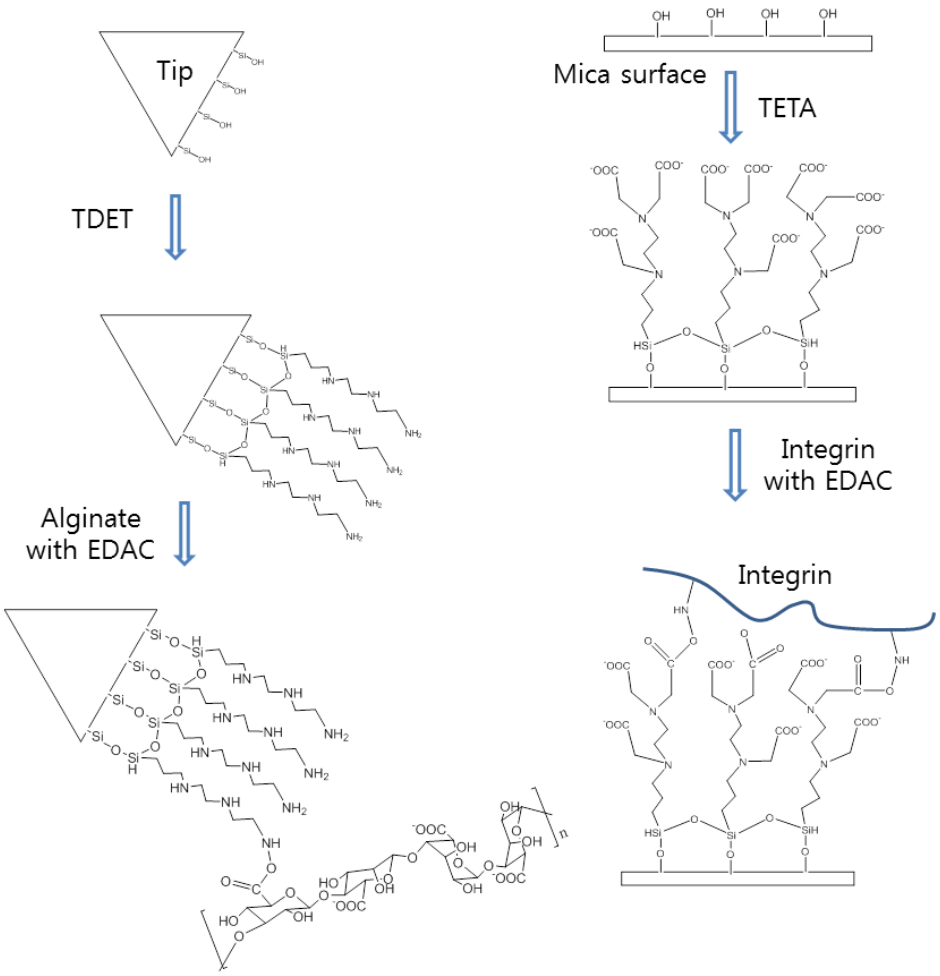

Figure 4.1. Steps of immobilisation of alginate and integrin
(RGD is not drawn on alginate)

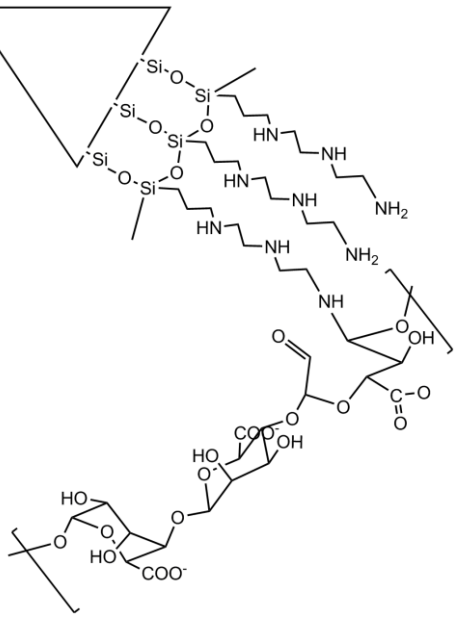

Figure 4.2. Result of reductive amination for POA
(GRGDYP are not drawn on alginate)

In order to prove the immobilisation, surface images were taken with multimode-AFM (Nanoscopella Digital Instruments, Santa Barbara, Ca). After the measurements, the surface was washed with MQ-water and dried with nitrogen gas followed by drying in a vacuum chamber.

4.3 Measurement

A JPK force robot ® 300 (JPK Instruments, Berlin, Germany) was used for the force measurement. The surface was glued on a Petri dish and was covered with filtered (0.2µm) HEPES (10mM, 4-(2-Hydroxyethyl)piperazine-1-ethanesulfonic acid, Sigma-Aldrich) buffer with NaCl (150mM), $MnCl_2$ (1mM) and $MgCl_2$ (1mM) in pH 7.4. Only the larger one of two cantilevers with silicon nitride tips (OTR4-10 Cantilevers, spring constant 0.02N/m, Au Reflective from Bruker AFM probes) was used. The spring constant was affected by degradation with the chemicals used during the immobilisation procedure and by the weights of the substrate bound to the tip and the cantilever. Therefore, the spring constant of each tips was calibrated before use by analysing the thermal fluctuations of the tip. The spring constant varied between 0.016

to 0.027 N/m. The deflection sensitivity of the system was also adjusted before every measurement, and occasional peeling of the gold coating was observed.

Measurements were carried out at a fixed loading rate (2.0μm/s). The extended delay time was adjusted between 0.1 to 0.3 seconds at constant-height mode. These adjustment were aimed at achieving around 10% interaction, according to the Bell-Evans theory [65].

As control experiments, silanised tip, silanised surface, POA tip, antibody surface and insulin surface were tested. The same silane chemicals and procedure were used as in section 4.2. For immobilisation of POA, antibody and insulin, carbodiimide chemistry was used. As there were several experiments with different condition and substrates, Table 2 summarises substrates on the tip and surface, and buffer used.

Table 2. Summary of buffer and substrates used for each experiment

Experiment	**In section**	**Buffer (concentration in mM)**	**Alginate used**	**Alginate Concentration (mg/ml)**	**Resting time (s)**	**Silane concentration and silanisation time**
Initial alg-GRGDSP and integrin	5.1	HEPES (10) NaCl (150) pH 7.4.	Alg-GRGDSP (FMC Biopolymer)	2 or 4	0.5 - 1.2	Tip : 3% 25mins Surface : 5% 25mins
Silane tip and silane surface interaction	5.3	HEPES (10) NaCl (150) $CaCl_2$ (1) pH 7.4.	-	-	0.1	Tip : 3% 1-30mins Surface 2-5% 10mins
Reactivity test of insulin with POA-GRGDYP	5.4	HEPES (10) NaCl (150) $MnCl_2$ (1) pH 7.4.	POA-GRGDYP (the first batch)	0.5	0.1	Tip : 1% 12mins Surface : 1% 12mins
Orientation and activation of integrin by using antibodies	5.5	HEPES (10) NaCl (150) $MnCl_2$ (1) $MgCl_2$ (1) pH 7.4.	POA-GRGDYP (the second batch)	0.6	0.3	

4.4 Analysis

Two programs were used for the analysis of the obtained force jumps. The JPK Data Processing program was used in order to view each individual force jumps and to manually filter out the graphs with interactions. Selected curves were converted into text files that were read by the force analysis program, ForceSpecAnalysev7.pro. The ForceSpecAnalysev7.pro was developed in IDL by Professor Bjørn Torger Stokke, NTNU, Trondheim.

4.4.1 Data collection

Curves with interactions were manually selected according to the following criteria

- Only jumps that started from the baseline were selected. The jumps indicated that a rupture had occurred in the polymer.
- Force jumps at the tip de-adhesion site were excluded. The first jump of the curve represents non-specific adhesion of the cantilever tip to the surface.
- The jumps should preferably be a single peak.

The selected force curves were converted into text files, providing information of the distance of the force jump that occurred at the deadhesion point, magnitude of the force jump from the base line and the corresponding loading rate for each force jump. The last analysis of loading rate for individual force was especially important because although the tip was moved at a constant loading rate, each de-adhesion occurred at a different loading rate, as the pulling speed was highly affected by the elasticity of the polymer [64]. The developed force analysis program “ForceSpecAnalysev7.pro” enabled a more detailed analysis of the force jump for polymer system.

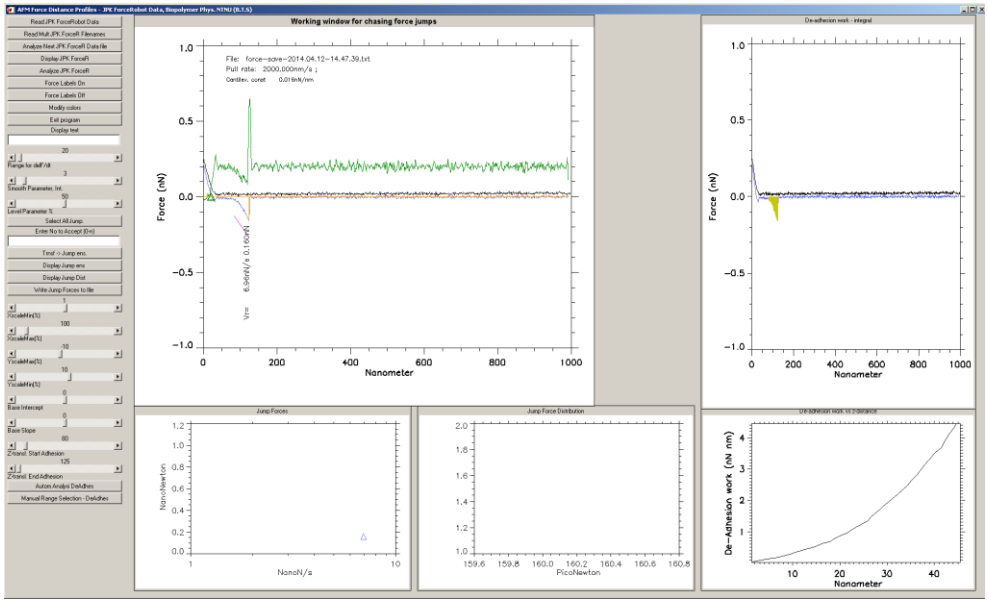

Figure 4.3. Screen capture of force analysis program (ForceSpecAnalysev7.pro)

4.4.2 Force jump analysis and Dynamic force graph

"DiForDisMultiJPK7.pro" was used to analyse the distribution of the magnitude of force jumps as the loading rate was analysed by the previous program (ForceSpecAnalysev7.pro). This program plots the unbinding force values against the log of the loading rate. According to Bell-Evans' theory, this distribution could be expected to give a positive linear relationship. The program also produces a histogram within a determined range of loading rate, giving the most likely magnitude of unbinding force for each loading rate. The program, in addition, calculates the curve fitting parameters of the distribution of the histograms generated for each loading rate. In this experiment, the reaction was not achieved, so the parameters were not calculated.

5 Results and Discussion

5.1 Initial alg-GRGDSP and integrin interactions

Alginate linked with GRGDSP (0.53%, calculation is provided in Appendix A) was investigated for interaction with integrin $\alpha_5\beta_1$. According to Bell-Evans' theory, 10% of interaction frequency ensures high probability (with ~95% confidence) of achieving single molecular bonds [65]. However, the system showed a very low interaction frequency (2.3%) as shown in Figure 5.1. Therefore, it can be concluded that there was no interaction between alg-GRGDSP and integrins.

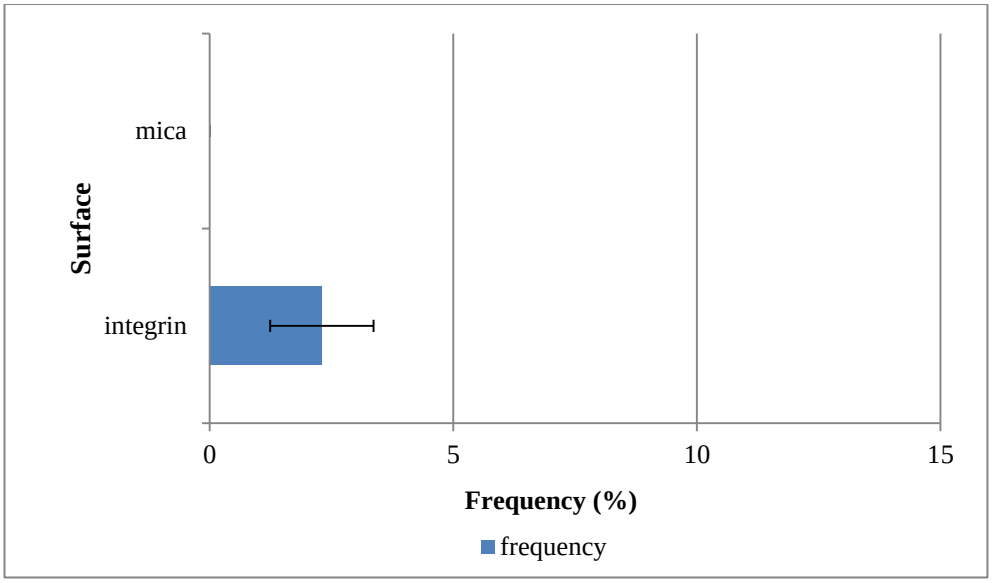

Figure 5.1. Alginate-GRGDSP and integrin interaction frequency
(Bases of the interaction counting found in Appendix C)

Three explanations can be given for such low degree of interaction. The first speculation is that there was no alginate immobilised on the tip. This is not likely, because in a previous alginate immobilisation experiment with the same protocol on the tip, 50 times less concentration of alginate was used for successful immobilisation. [67]

The second speculation is that the integrins were not properly immobilised on the mica surface. Either areas of silanised mica surface was left uncovered, or the head parts of

integrins (where RGD binds) were not positioned upwards. AFM was used for imaging the integrin-immobilised surface, as shown in Figure 5.2. The AFM image showed that the mica surface was completely covered with some particles that are suspected to be integrin molecules. The closed up image (Figure 5.2 (b)) showed a shape that can has similar shape to integrin; the dimer molecule seems to have two head parts and a long body. The length of the molecule is approximately 25nm and it corresponds to the known heights of an integrin dimer, which is 19nm [36]. Thus, the conclusion is that the molecules imaged by AFM were integrins. Higher resolution of the image could have confirmed that the molecules were indeed integrins, however such procedure was not appropriate at the stage as there were technical complications with the instrument, and it was hard to optimise for the highest possible resolution.

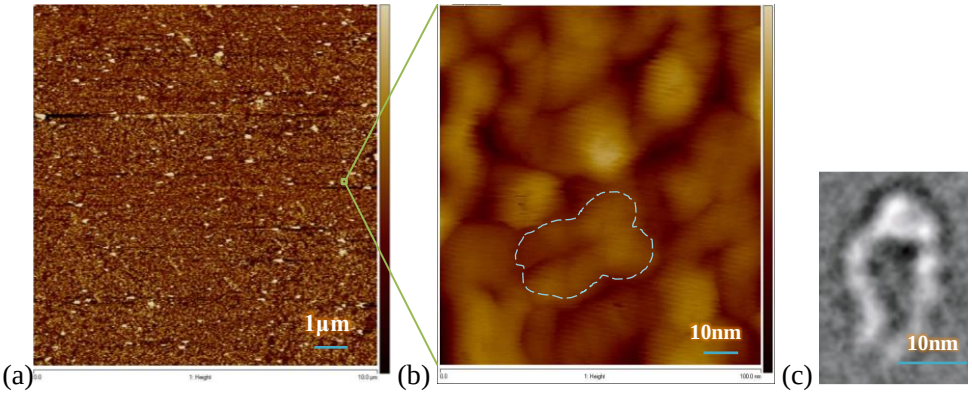

Figure 5.2. AFM image of integrin immobilised on mica surface.
(a) 10µm x 10µm of integrin surface. 100 points from this size of area was used for the measurement of integrin and alginate interaction. (b) Magnified integrin surface. The molecule with the length indicated is likely to be an integrin molecule as the length and the shape of the structure corresponds that of integrin molecules known. (c) electron microscopy image of extended integrin taken from M.Humphries et al. (2003) [68].

As integrins seemed to cover the mica surface, there is uncertainty whether integrin were properly oriented. Integrin binds to its ligands only when the ligand-binding site of the integrin is exposed and oriented so that it can readily catch the ligands. The ligand binding site is located at an interface between the head part of α_5 and β_1 subunits [36]. Therefore, it is important that the heads of the dimer are oriented upwards. This is

achieved in cells naturally as the rod-like legs are located within the bilipid layer, exposing the head part over the membrane. However, for this measurement, a carbodiimide chemistry was used for the immobilisation of integrins to the silanised mica surface. The reagent could make covalent bond with any amine groups available on the integrin surface (Figure 4.1). Therefore it can be assumed that a large percentage of the integrins were not properly head-up oriented. This argument can be supported by the work of D.Nordin et al. (2012) who described that when integrin were spontaneously adsorbed on the mica surface, the integrins were lying flat and did not show any interaction with fibronectin [69]. In Figure 5.2, the highlighted integrin was also lying horizontally on the surface and this could be the case for most the other integrins. Therefore, another procedure was required to control the orientation of integrins during the immobilisation steps. This is further discussed in Result and Discussion 5.5.

The last speculation is that the immobilised alginate chain did not contain grafted GRGDSP that could efficiently interact. It was calculated in Appendix A, that the alg-GRGDSP had a DP (degree of polymerisation) of approximately 1100, and 0.53% of monomers werecoupled with peptides. Therefore, in average, one polymer chain was likely to have five of the hexapeptides grafted. This is not a high enough number of peptides to achieve frequent interactions. Moreover, the coupled RGD was randomly distributed, and if the grafted peptides were located near the tip, the interaction would not be likely to happen due to hindrance by the tip. Even though the RGD near the tip managed to interact with integrin, the resulted force jump was likely to be masked by the larger force jump caused by the deadhesion of the tip from the surface.

In order to confirm interaction between grafted RGD ligands and integrins, it was required to make sure that there was a high enough number of RGD peptides grafted on the alginate. The carbodiimide chemistry method has shown to give a relatively low grafting level. For example, a coupling rate of 0.2~0.3% was achieved, when 5% by mass of GRGDYP was available [42]. Therefore, carbodiimide chemistry was not regarded as the appropriate coupling method to use for further experiments. Thus, another coupling method was sought. Periodate oxidised alginate (POA) has been shown to have a much higher coupling rate as the number of reactive functional sites can be created by oxidation, and up to half of the functional sites are available for further coupling [45, 48]. Therefore, it was decided to substitute the carbodiimide cross-linked alg-GRGDSP with POA-GRGDYP. The GRGDYP hexapeptide was

chosen to be coupled because it has shown cell capturing ability [70]. The result of GRGDYP grafting on POA is presented on the following section (Result and Discussion 5.2).

5.2 GRGDYP coupling to POA

As discussed on Results and Discussion 5.1, RGD-containing-hexapeptide (GRGDYP) was grafted on POA. Two different alginate precursors were used. Both of the alginate, batch no.1 (Mw = 103300g/mol) and no.2 (Mw = 271000g/mol), were first oxidised with sodium periodate aiming 8% of oxidation, and followed by GRGDYP coupling by reductive amination. The second batch consisted of alginate with three times higher molecular weight in order to obtain longer chains. H^1-NMR analysis and calculation of the degree of coupling is provided in Appendix B.

Table 3. GRGDYP coupling rate to POA

Batch no.	Oxidation (%)	GRGDYP Coupling (%)
1	8	4.8
2	8	5.5

In this experiment, 4.8% and 5.5% of coupling was achieved based on an optimised protocol from Marianne Øksnes Dalheim (not published). This is approximately 10 times higher coupling efficiency than when using carbodiimide chemistry where 0.5% grafted monomers is obtained.

The RGD-coupled alginate sample used at the previous experiment (Results and Discussion 5.1) was calculated to have approximately five RGD-coupled monomers per chain. The number of the peptide-coupled monomers per chain increased significantly by using periodate oxidation and reductive amination method; in average, batch no.1 achieved 13 RGD-coupled monomers per chain and batch no.2 obtained 42 coupled monomers per chain (Calculation found in Appendix B).

Even higher coupling rate could have been achieved with longer reaction time. However the longer the reaction time is, the higher degradation of the polymer chain is. This is because free radicals can be formed by the reducing reagent, and

depolymerisation by free radicals can occur[44]. In addition, the mild acidic condition can further accelerate the hydrolysis of alginate. In order to reduce degradation in this experiment, 1-propanol was used to mitigate extent of polymerisation [71], oxygen was removed to avoid free radical formation, and reaction was carried out at a low temperature (4℃). Nevertheless, the chain length could have been reduced and consequently chain flexibility would increase. For such reason, it is recommended to test the molecular weight and viscosity again in order to gain insight into the properties of alginate before it is used for single molecular force analysis.

5.3 Silane tip and silane surface interaction

From previous experiments (data not shown), silane tip and silane surfaces showed high level of interactivity with substrates. Silane is expected to form a monolayer assembly covering the tip surface or mica surface, and no interaction was expected. Nevertheless, a polymer-like interaction was observed, so that the silane-silane interaction was further analysed.

Figure 5.3 shows an interaction between the silane surface and the silane tip. For the tip, three variables were used: no silane tip (0 silanisation time), 10 minutes silanised tip and 30minutes silanised tip. For the surface, the concentration of silanes was varied while the silanisation time was equal for both of the surfaces. A difference was observed: silane tip and silane surface showed a high frequency of peeling reactions (force jump curves with single to multiple plateaus) of up to several hundred nanometres, whereas the tip without any silane showed almost no peeling reactions but mostly force jumps in relatively high frequency. The typical peeling reaction profiles are shown on Figure 5.4.

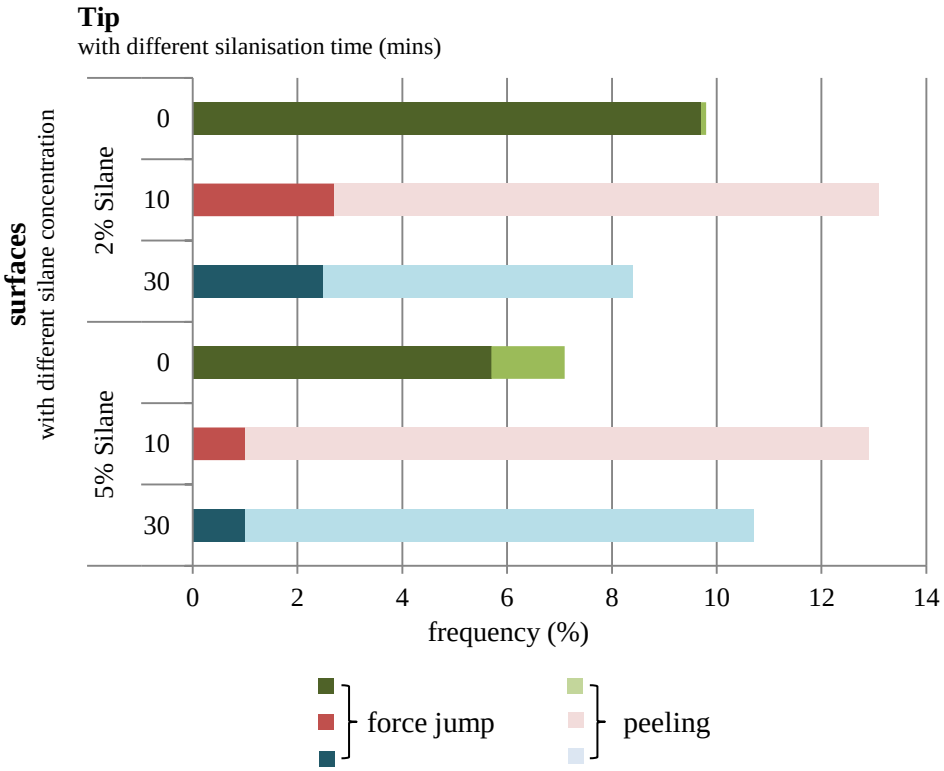

Figure 5.3. Silane surface and silane tip interaction frequency

Silane surfaces were treated with different concentration of silane (TETA). Silane tips were treated with different silanisation time while all of the tips had the same concentration (3%) of silane TDET. The darker colour indicates force jump, while the lighter colour indicates peeling events. (Standard deviation could not be calculated as the graph is based on one set of measurement. Base of the interaction counting is provided at Appendix D)

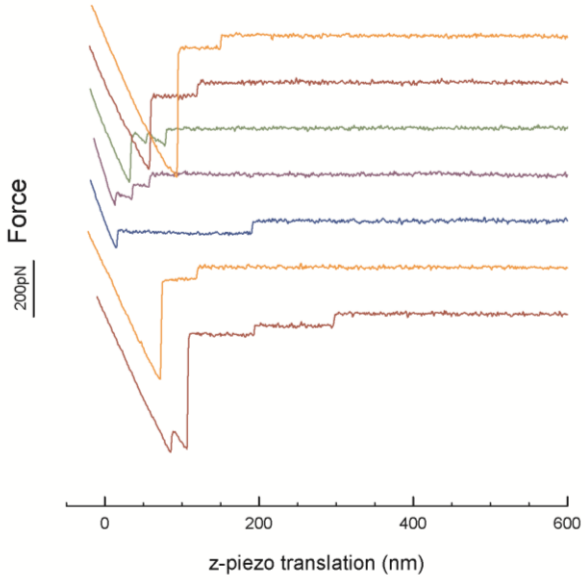

Figure 5.4. Gallery of typical interactions of silane surface and silane tip
Length of plateau of the peeling events occurred at the each of the silane-silane combinations in Appendix E.

A peeling reaction is caused by a series of weak attachments of the two substrates, and as the tip is retracted, a long polymer is peeled away as shown in Figure 5.5. Therefore, two criteria must be fulfilled to obtain peeling reactions: there must be a polymer in the system, and the polymer should interact with the surface. The latter was fulfilled, as TETA, contains carboxylic groups that are charged negatively in the neutral solution, while a TDET molecule has three positively charged amine groups in its end at pH 7. The buffer in pH 7.4 was used, thus during the measurements, the oppositely charged two silane molecules could have ionic interactions between the carboxylic groups and the amine groups.

However, the former criteria should not have been satisfied, as alkoxysilanes (e.g. TETA and TDET) are self-assembly molecules that ideally form a horizontal single layer parallel to the mineral surface. The single layer plays a role as a connector between the surface and organic molecules by forming covalent bonds. Therefore, no peeling reactions were expected, because no polymer should exist in the system. However, up to 500nm of peeling reactions were observed, as shown in Figure 5.5

(analysis for distribution of the length of the plateaus is provided in Appendix E). The length of the plateaus can be assumed to be equal to the length of the polymer that the tip pulled away. Therefore, this result indicates there was polymer in the system, and this can be explained by several reasons.

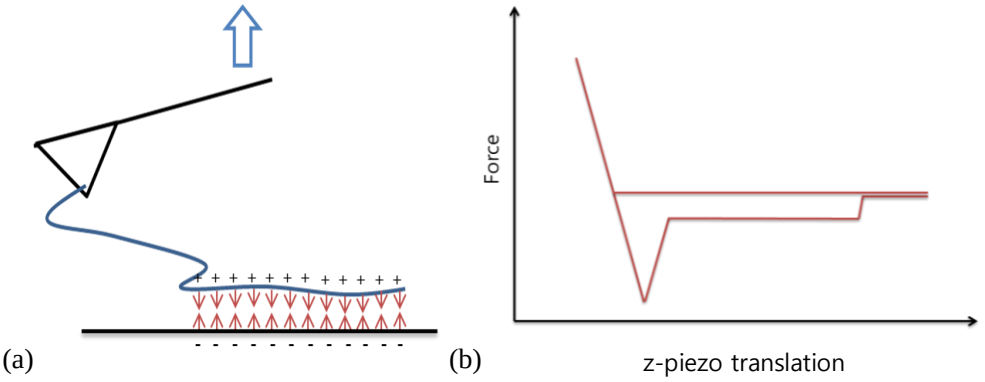

Figure 5.5. Peeling reaction
(a) The tip is lifted and the small interaction (for example ionic interaction as shown) between the polymer and the surface is ruptured. (b) A typical profile of a peeling event.

First, there could have pollutants added to the system during the silanisation steps causing immobilisation of the pollutant particles. However, this is highly unlikely, as ultrapure MQ-water was used as solvent and all the solutions used were filtered using a 0.2µm filter before the use.

Secondly, vertical polymerisation of the TETA and TDET can be questioned. It is known that silanes can undergo not only horizontal polymerisation, but also vertical polymerisation, depending on the silanisation conditions [72]. T.Baumgartel et al. (2013) have investigated that the Si-O-Si bond formation occurs not only between the OH groups on the mineral surface and Si of silanes, but also among silanes (octadecyltrichlorosilanes) in the presence of excess water on the surface [73]. The vertically formed silane chains generated clusters of silane of up to 100nm in length [73].

In order to prevent vertical polymerisation of silanes, low humidity and high density of exposed hydroxyl group on the mineral surface have been recommended [73]. A.Y.Fadeev et al, also argued that sufficient amounts of water in the system could cause polycondensation of trifunctional silanes into vertically polymerised structures [72]. Low humidity seems to be required in order to avoid vertical silanisation. It can be achieved by performing the silanised reaction in an organic solvent (e.g. toluene) in a glove box where any water vapour is completely removed [74].

Moreover, a low concentration of silane is important. It was reported that a 0.25% silane solution on a glass surface could result in three to eight layers of either interconnected or loosely connected assembly of silanes [75]. In this measurement (Figure 5.3), 3.0 to 5.0% silane solution was used. Therefore, further dilution of the silane is recommended in order to achieve single layered silane.

As the implementation of organic solvent was difficult, the concentration of the silane chemicals was reduced down to 1.0% for the further investigation. The silanisation time was also reduced down to 10 minutes. However, more information about the kinetics of self-assembly of silane is required in order to support the efficiency of the reduced silanisation time for vertical polymerisation.

Finally, it was suspected that the polymerisation of silane had already occurred by the humidity inside bottle used in this study as the bottle is several years old and had been opened many times for previous experiments.

Above all, polymerisation of silane will not be a very much concern as far as complete coverage of proteins on the silane surface is achieved. The same silanisation coating procedure has been used by M.Sletmoen (2004) [67], and no significant noise from silane was observed. As a conclusion, the significance of vertically polymerised silane structures will be small with a silane surface properly covered with substrate.

5.4 Reactivity test of insulin with POA-GRGDYP

Interaction between the alginate tip and the insulin surface was measured in order to test the use of insulin as a non-interactive blocking material for alginate. Insulin is known to be non-reactive with alginate when measured with Isothermal Titration Calorimetry (ITC) [76]. However, the insulin surface showed slightly higher reactivity than the integrin surface with POA-GRGDYP as shown in Figure 5.6.

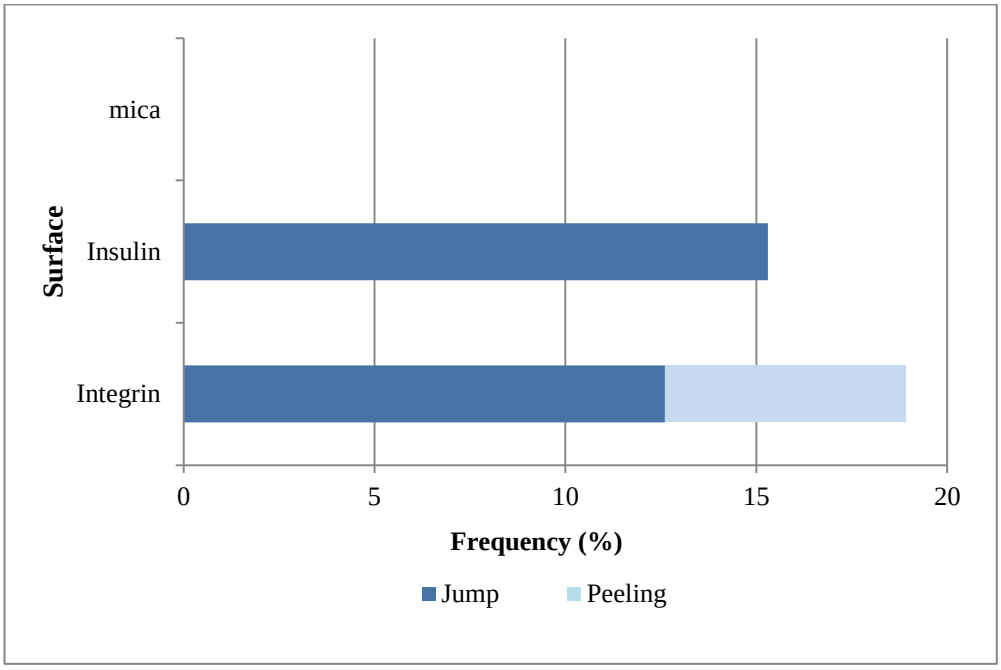

Figure 5.6. Frequency of interaction between POA-GRGDYP and insulin surface and integrin surface

Comparison between Insulin surface and Integrin surface with the same POA-GRGDYP tip. (Standard deviation could not be calculated as the graph is based on one set of measurement. Base of the frequency count is provided at Appendix F)

This result means that either 1) the insulin was as interactive as integrin with POA-GRGDYP, or 2) neither the insulin nor the integrin was specifically interactive with POA -GRGDYP.

The first argument is less likely. This is because the surface of insulin is negatively charged in neutral solution and alginate is a negatively charged polysaccharide [76]. However in Kristoffersen's study, pure alginate was used for the interaction test [76],

while in this experiment alginate was oxidised and coupled with the hexapeptide. By oxidisation, alginate gains higher flexibility than intact alginate, increasing the possible contact area to the surface of other molecules [71]. Apart from the flexibility of the alginate, the hexapeptide molecule contains positively charged side chains that could have interacted with insulins. As the number of monomers in the alginate coupled with hexapeptide is significantly high (4.3% of this first batch) this interaction could have been reflected in the force curves.

The measurement technique could have contributed to the different result. Although both ITC and AFM can measure protein-protein interactions, they have different approach and limitations. In ITC sample molecules can diffuse freely and their value limits as average values of interaction. On the other hand, AFM measures the direct force exerted from single-molecular deadhesion, and the molecules move in one dimension (up and down) [77, 78]. In addition, AFM is much more sensitive method than ITC, as it does not only give information about affinity, but also information about the binding profiles and binding energy barrier, which can be calculated from AFM data. Thus, interactions that was not measured by ICT could have been detected by AFM. .

The second argument, neither the insulin nor the integrin was specifically interactive with POA –GRGDYP, is difficult to support due to the high (about 10%) level of interaction frequencies in the Figure 5.6. Such high interactions could have been the result of unspecific interactions between the silane surface and POA-GRGDYP. Silane that was not covered by proteins could have caused the force jumps.

In conclusion, it is recommended to run another test with higher concentration of insulin on the surface to ensure complete silane coverage. If high insulin interaction is still observed, another blocking material should be used. BSA (Bovine Serum Albumin) which is commonly used as a blocking material, has shown interaction with alginate on ITC [76], so that other molecules are needed to be investigated. Any molecules that are highly negatively charged are recommended, as they would be expected to repel the negatively charged alginate.

5.5 Orientation and activation of integrin by using antibodies

The aim of this experiment was to control the orientation of integrins so that the head domains were projected upwards. Moreover, a new batch POA-GRGDYP with longer alginate (batch no.2: Mw = 271000g/mol, 5.5% coupling) was used in this experiment as it was desired to obtain force jumps further away from the deadhesion of tip than for previous experiments.

Three methods were found to immobilise integrins with controlled orientation for AFM dynamic force measurement; F.Kong (2009) used truncated and Fc-fused integrins that contains only head groups (Figure 5.7 (b)) [79], while D.Nordin (2012) used supported lipid bilayer (SLB) to mimic the cell membrane by embeding integrins [69]. The possibility of using truncated integrins was discarded as transmembrane-truncated integrins were not purchasable. Formation of SLB was excluded, as it required expertise to generate stable SBL. Even though stable SLB could have been generated, there was high risk of pulling the integrins out from the SBL during measurements.

F.Kong (2009) captured integrins by using antibodies as shown on Figure 5.7 (a) [79]. In his study, the end of the cytoplasmic domain of integrin was fused with Fc proteins and was captured by anti-Fc antibody. Since diverse antibodies for integrins were available, the method of antibody capturing was implemented. Unlikely F.Kong, pure integrins were used (without Fc domains), since there was a lack of the recombinant genes for Fc-fused integrins and time constrains for the material preparation. Therefore, antibodies that could capture integrin were investigated.

CD29 (β_1) antibody was selected due to the following reasons. First, it does not compete with RGD for the binding site. Second, it immobilises β_1 subunit, which is more directly involved in RGD capturing [80]. In addition it was reported that the CD29 (β_1) antibody has activating influence on the β_1 unit, as it straightens the conformation of the β_1 subunit into the activated state regardless of the existence of ligands [81].

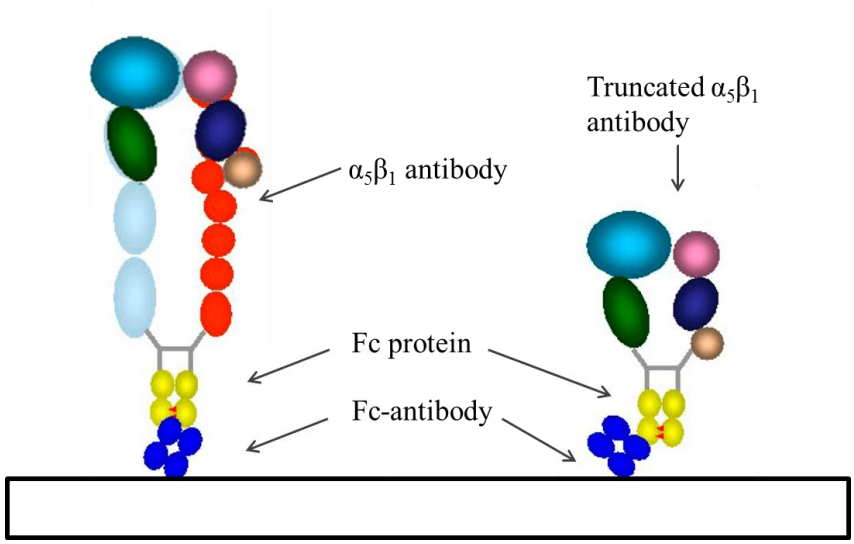

Figure 5.7. Fc-Integrin captured by anti-Fc proteins
Reproduced from F.Kong (2009) [79].

However the downside of the CD29 antibody is that it does not capture the cytoplasmic end of the integrin, but rather the rod-like domain of integrins (It has not been specified exactly which sequence of integrins it binds) [82]. Therefore, the integrins might not completely straightened when they were captured. Furthermore, the activating effect was only studied for $\alpha_4\beta_1$ and integrins on prostate cells (subunit combination was not specified) according to P.Sainchez-Aparicio's work (1994) [81]. In addition, no information regarding the strength of the bond between the antibody and integrin has been characterised. If the antibody-integrin bond is weaker than integrin-RGD bond, AFM would measure the rupture force between antibody and integrin rather than the integrin and RGD. For these reasons, it needs to be studied the effect of antibody CD29 on the purified integrin $\alpha_5\beta_1$, and its binding strength to its antigens. All these factors may be the reason for which capturing the integrins with an antibody did not improve the interactivity of integrins.

For this section, a more detailed force analysis was used. In the previous experiments the interactions were divided into force jump reaction and peeling reactions. In this section, the force jump reactions were categorised into two types: force jumps below 500pN, and above 500pN. This is based on the review from J.Zlatanovaa, showing that avidin and biotin gave approximately 100 to 200pN average forces [83]. As avidin and

biotin are known to have the strongest non-covalent interaction found on a biological system [84.], interactions between single integrins and RGDs POA-GRGDYP interaction were unlikely to exceed 500nN.

In order to produce statistically significant data, two experiments with the same set of molecules were combined for the data presented on the Figure 5.8. Figure 5.8 show that peptide-blocked integrin had the same level of interaction as integrin (non-blocked). Therefore, it can be concluded that no specific interaction was observed between integrins and POA-GRGDYP.

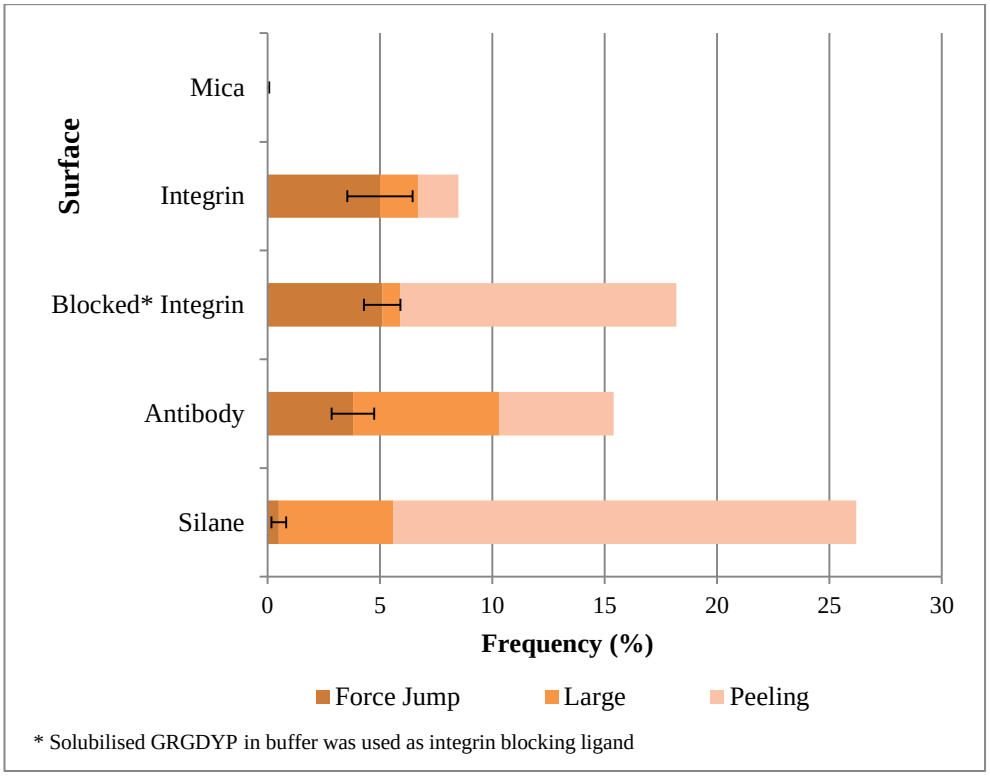

Figure 5.8. Frequency of interaction between POA-GRGDYP and different surfaces
Surfaces tested were $\alpha_5\beta_1$ integrins captured by antibody CD29, GRGDYP blocked integrin (captured by antibody), antibody CD29, and silane. (Base of the frequency is provided at Appendix G)

There was interest to investigate whether there is any differences among the surfaces with the similar frequencies. Thus, detailed analysis of each force curves from different surfaces were analysed using force analysis program. For each surfaces, the

distribution of force jumps were presented against increasing loading rate. A histogram of the forces (Figure 5.9 (b)) shows the most likely forces at the loading rate of 2.0 nN/s. A gallery of representative force jump curves (Figure 5.9 (c)) was generated.

5.5.1 Integrin captured by antibody on surface and POA-GRGDYP on tip

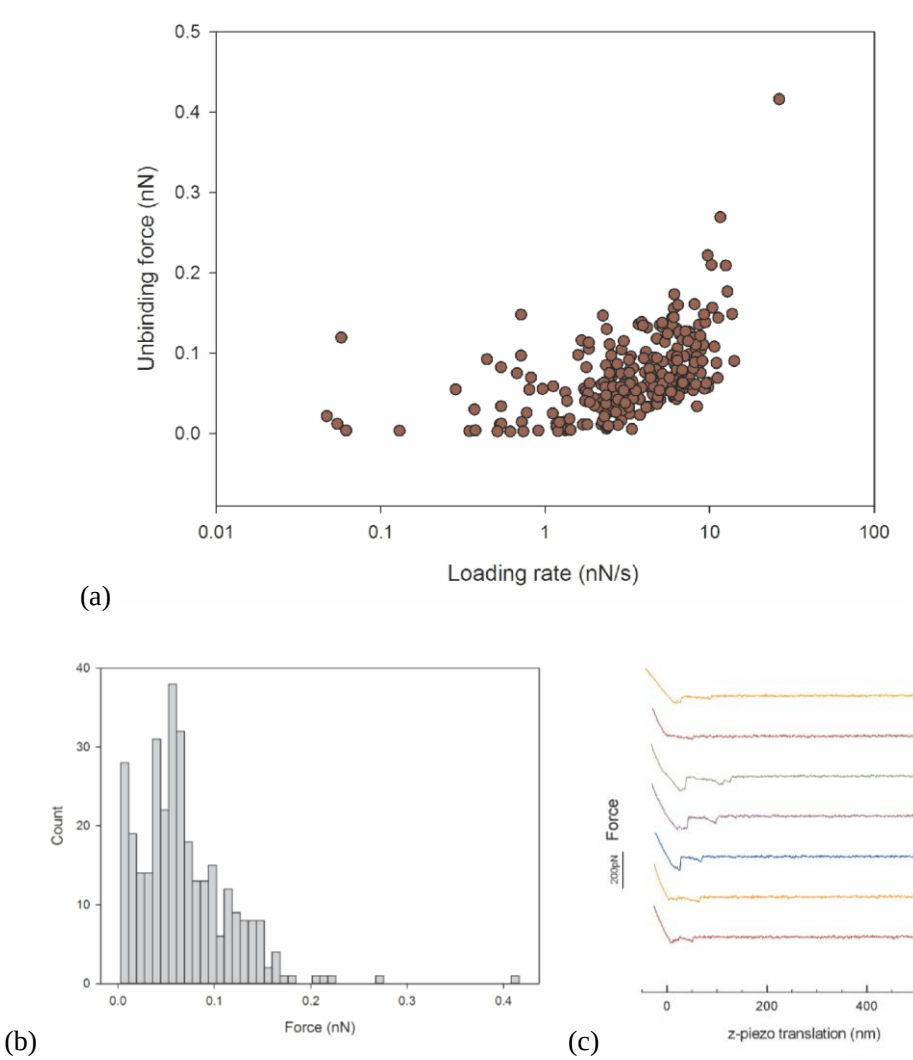

Figure 5.9. Integrin captured by antibody with POA-GRGDYP

(a) Distribution of unbinding forces were plotted as a function of variabilities in loading rate at a set speed of cantilever was 2.0nN/s on the JPK force robot. (b) Histogram of unbinding forces. (c) Gallery of representative force retraction curves.

5.5.2 GRGDYP blocked Integrin on surface and POA-GRGDYP on tip

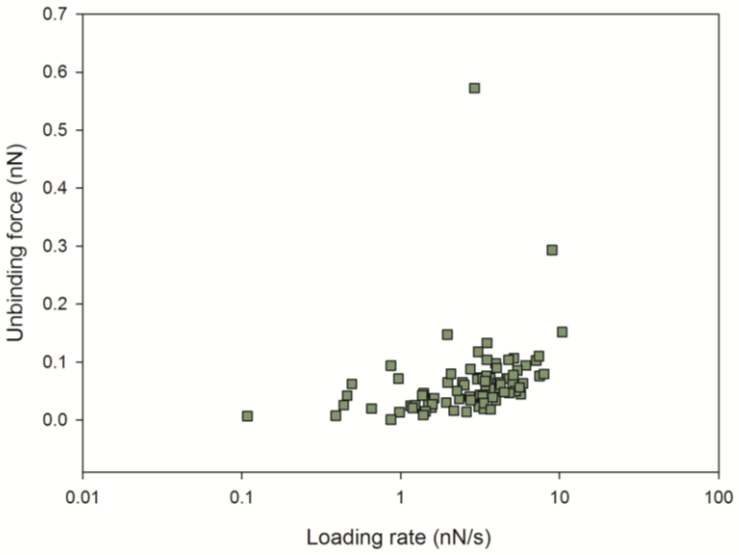

(a)

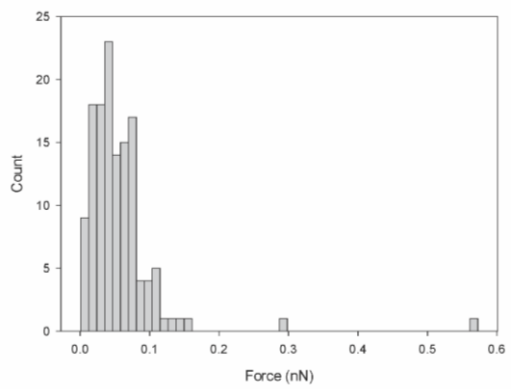

(b)

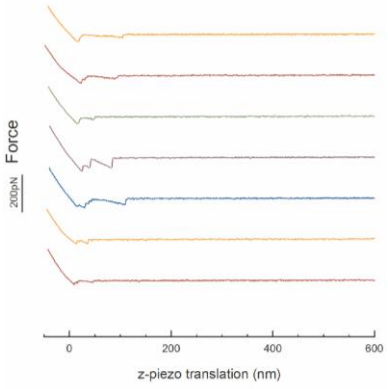

(c)

Figure 5.10. GRGDYP blocked integrin (captured by antibody) with POA-GRGDYP
(a) Distribution of unbinding forces were plotted as a function of variabilities in loading rate at a set speed of cantilever was 2.0nN/s on the JPK force robot. (b) Histogram of unbinding forces. (c) Gallery of representative force retraction curves.

5.5.3 Antibody on surface and POA-GRGDYP on tip

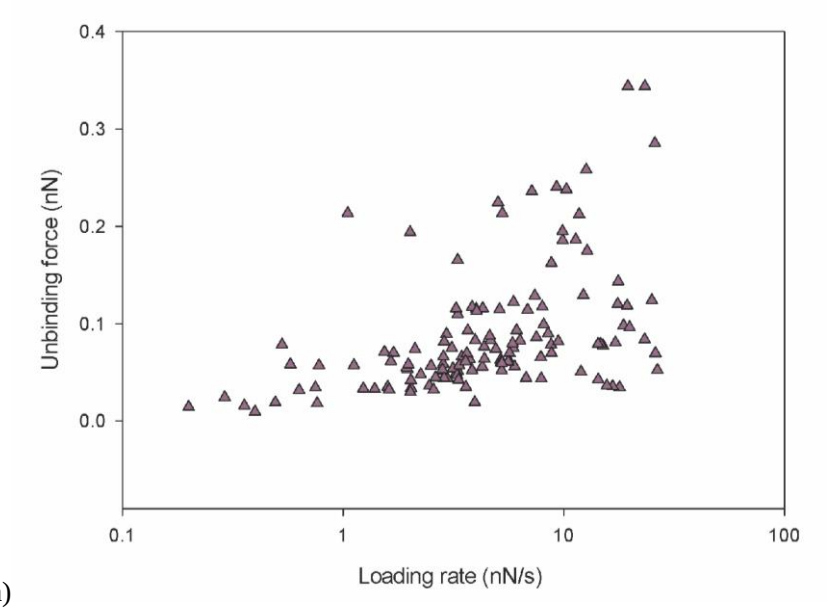

(a)

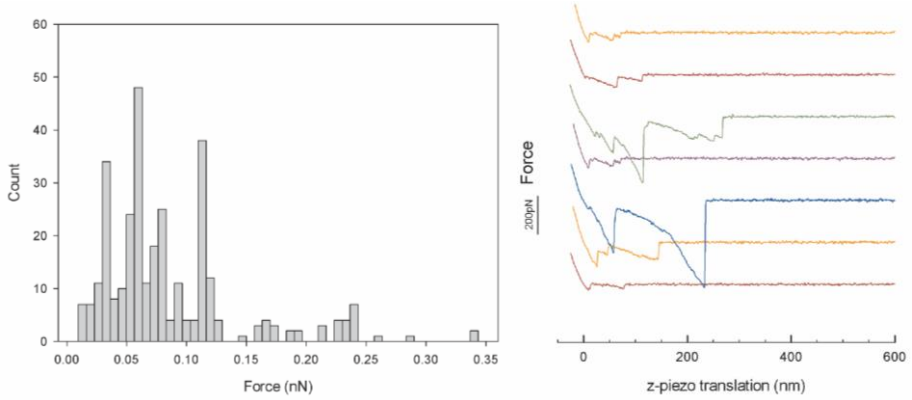

(b) (c)

Figure 5.11. Antibody with POA-GRGDYP

(a) Distribution of unbinding forces were plotted as a function of variabilities in loading rate at a set speed of cantilever was 2.0nN/s on the JPK force robot. (c) Gallery of representative force retraction curves.

5.5.4 Silane on surface and POA-GRGDYP on tip

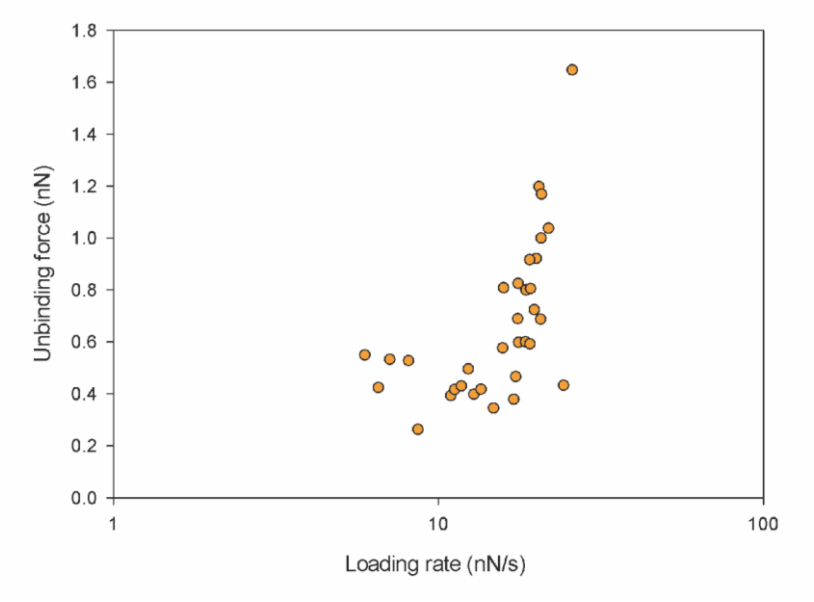

(a)

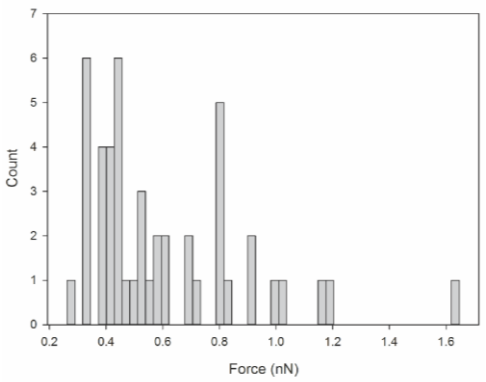

(b)

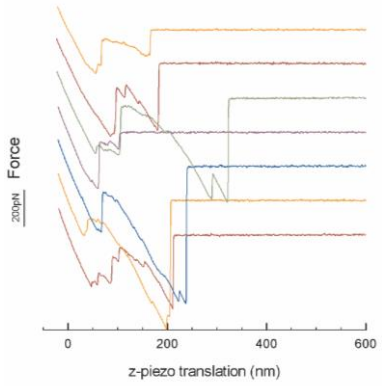

(c)

Figure 5.12. Silane with POA-GRGDYP

(a) Distribution of unbinding forces were plotted as a function of variabilities in loading rate at a set speed of cantilever was 2.0nN/s on the JPK force robot.. (b) Histogram of unbinding forces. (c) Gallery of representative force retraction curves.

5.5.5 Comparison of all the surfaces

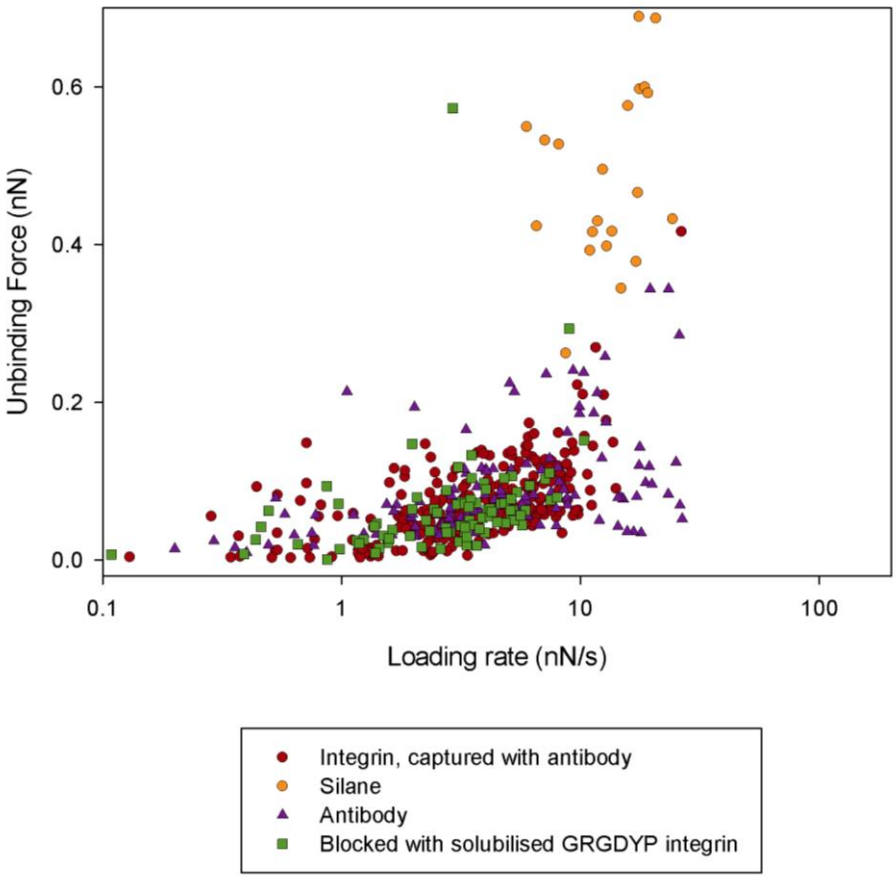

Figure 5.13. All surfaces with POA-GRGDYP
Distribution of unbinding forces were plotted as a function of variabilities in loading rate at a set speed of cantilever was 2.0nN/s on the JPK force robot.

Figure 5.13 shows that the distribution of three set of measurements (‘Integrin, captured with antibody’, ‘Blocked with solubilised GRGDYYP integrin’ and ‘Antibody’) had a similar distribution within the same range of loading rate, while the measurement with ‘Silane’ had a different distribution of unbinding force and different range of loading rate. Therefore, it can be concluded from Figure 5.13 that there was

no specific interaction, since POA-GRGDYP had the same type of reaction with the different integrin surfaces (regardless of whether it was blocked or not) and antibody surfaces.

The argument that integrin surface and blocked-integrin surface showed no significant difference can be supported in the detailed force analysis in the Figure 5.9 and Figure 5.10 by comparing histograms of force distribution and profiles of the force retraction curves. From the two histograms (Figure 5.9 (b) and Figure 5.10 (b)), the similar values of the most likely force were detected (0.55nN and 0.45nN respectively) and a similar distribution shape (sharp bell shape) of force was observed.

Although the antibody had similar distribution of force jumps vs loading rate compared to the integrin surfaces in Figure 5.13, the antibody surface showed wider distribution histogram (Figure 5.11(b)), and the some of the force retraction curves (Figure 5.11 (c)) were larger in the magnitude of force jumps than the curves of the integrin surfaces. This tells that the antibody surface have different properties compared to the integrin surfaces, however antibody surface is still interactive with POA-GRGDYP.

Finally, the distribution of silane force jumps were much wider (Figure 5.12 (b)) and the force retraction curves showed much larger peaks (Figure 5.12 (c)) than the other systems, indicating the silane surface has much stronger interaction with POA-GRGDYP.

In conclusion, integrins did not show any specific interactions towards POA-GRGDYP. There may be a numbers of reasons for why the interaction was not observed in this experiment. Before discussing the arguments, it is important to emphasise that interaction between POA-GRGDYP and immobilised integrins should be tested with different measurement techniques. If there is interaction between the two proteins, the measurement technique needs to be modified. If there is no interaction, the proteins are either denatured or non-functional. ITC is recommended since it is less expensive than AFM, and the most quantitative method for measuring thermodynamic properties of protein-protein interaction [85].

5.5.6 Functionality of POA-GRGDYP

A speculation can be casted whether the GRGDYP was active or not. Unlike carbodiimide coupled alg-GRGDYP by K.Karstensen, 2010 [86], no data for cell

viability is available for POA-GRGDYP coupled by reductive amination due to its early stage of research.

Side reaction on the hexapeptide may arise during the carbodiimide reaction for the immobilisation stage. The peptide has two carboxylic groups: one on aspartic acid and the other one on the proline end of the peptide. These carboxylic acid groups might react with EDAC and form a covalent bond with amine groups on the tip, leaving less available peptides [87].

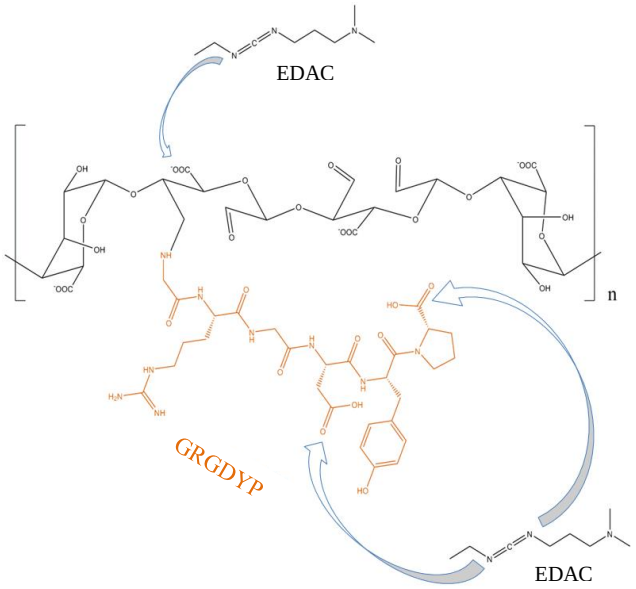

Figure 5.14. Possible carbodiimide chemistry bond formation site by EDAC
The arrows indicate the EDAC attacking site on alginate. The carboxylic groups on the alginate backbone are desired to react with EDAC whereas those on the peptides are to be avoided.

For further experiment, changing the structure of the RGD-peptide can be suggested in order to increase the affinity of the grafted peptide. Integrin showed very different binding affinity towards RGD depending on the surrounding peptides around the RGD. For example E.Koivunen (1994) showed in their binding assay with various peptide phages that the cyclic peptide GA*CRGDC*LGA showed a 10 fold higher affinity for $\alpha_5\beta_1$ than the linear RGD peptide sequence, GRGDSP [88]. Inserting RGD within a β

turn of protein structure is also recognised as a method to increase functionality of RGD [89].

5.5.7 Functionality of integrin

If the functionality of POA-GRGDYP was not the factor that inhibited the system from interacting, then the functionality of integrins can be questioned. Three aspects can be considered: conformation of integrins, stability of bimolecular unit and activity level of the biding site for RGD.

It is not known the conformation of integrin during the measurements. Integrin is known to have two conformations (Figure 3.7); bent (inactive) and straight (active), and divalent ions are known to be essential for stabilising the conformation of integrin. According to P.Mould et al. (1995), ligand binding activity of integrin $\alpha_5\beta_1$ had drastically increased with up to 1mM of Mn^{2+} and Mg^{2+}, whereas Ca^{2+} inhibited ligand binding [37]. Another study has shown that highest activity of integrins was shown at 10mM of Mn^{2+}, while Ca^{2+} reduced the binding activity [90]. S.Tiwari et al. (2011) supported this argument saying that Ca^{2+} has a main role in integrin folding and assembly within the cell, so that integrins stay inactive form until they reach the cell surface [38]. The buffer used in this experiment contained both Mn^{2+} and Mg^{2+} for the measurements shown in the Result and Discussion 5.5. However, the conformation of the integrins was not investigated. For example, trace of Ca^{2+} could have reduced the number of active integrins available.

The second aspect is the stability of the integrin subunits. An integrin protein consist of two non-covalently bound subunits to each other [91]. It has not been identified whether the integrins exist in the heterodimer form when it is immobilised on the mica surface. In several papers, recombinant integrins with dimer forming domains were used in order to achieve heterodimer position. J.Takagi (2003) and M.Nagae (2012) have used recombinant integrin with 30-residue ACID-Cys peptide and 30-residue BASE-Cys peptide and hexahistidine tag which form disulphide-brideged helical coiled coil conformation (called clasp) [33, 92]. A.Coe (2001) have used recombinant $\alpha_5\beta_1$ that were fused with Fc domains in order to form a stable heterodimer formations because the Fc domains form disulphide links between them [93].

However, integrins without any fused functional sequence for immobilisation have also been implemented for $\alpha_V\beta_3$. DH-Sepharose 4B resin coated beads were used as a solid

support and the rest of unacted immobilisation site were blocked with ethanolamine. From Greenberg et al.'s study (1999), they concluded that 35% of the immobilised integrins were active [94]. Since this study showed that immobilisation of pure integrins still maintains some level of integrin activity, the immobilised $\alpha_5\beta_1$ used for the measurements in Figure 5.8 is assumed to maintain certain level of interactivity towards RGD ligand.

The last aspect concerns whether that the activity of integrin's binding site was reduced or not, during the immobilisation steps. The effect of EDAC can be ranged from conformational change up to complete protein denaturation [95]. P.Lee et al. (1993) have demonstrated the destructive function of EDAC on enzymes during the carbodiimide immobilisation procedure. They minimised the destructive function of EDAC by first activating alginate and then removing excess EDAC with acetic acid, and subsequently the enzymes were added to immobilise [96]. Therefore, possible reduction in binding ability during the immobilisation stage should considered when it comes to the issue of achieving high activity of integrins, when performing force spectroscopy.

Nevertheless, it should be taken into account that EDAC is a commonly used reagent for the carbodiimide reaction, and it has been used widely used for the immobilisation of enzymes when testing their activity by force spectroscopy (e.g. M.Sletmoen's study in 2004 [67]). Therefore, the effect of EDAC on the integrin, specifically on the RGD binding site, should be further investigated.

5.5.8 Specificity of integrin towards RGDs on alginate

It can be questioned whether $\alpha_5\beta_1$ integrins can efficiently bind to RGDs on alginate. Under the assumption that the integrin had difficulties to interact with RGD that are coupled on alginate, three hypotheses can be suggested.

The first hypothesis is that integrin has very large groove near the binding site and alginate is relatively too thin and too flexible to completely fit into the groove. Consequently, alg-GRGDYP might bind to the groove independent of the RGD binding site. For instance, alginate can wrap around the integrin (as its flexibility increased after oxidation) or it can fit within the groove of integrin where fibronectin would be expected to bind, forming an energetically stable bond, without RGD binding.

Figure 5.15 shows the difference between integrin with alginate chain and fibronectin chain.

(a) 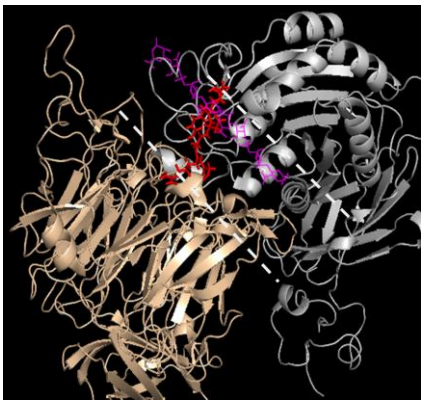 (b) 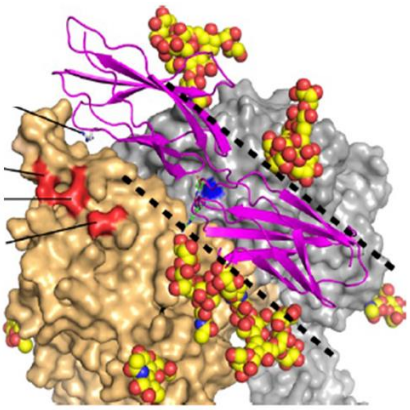

Figure 5.15. Comparison of binding on integrins between RGD-coupled alginate and fibronectin

(a) Integrin α_5 (wheat) and β_1(grey) with RGD(red)-coupled alginate(purple), reproduced by PyMol from Integrin $\alpha_5\beta_1$ (PDB ID : 3VI4) modified from M.Nagae (2012) [33]. (b) Integrin α_5 (wheat) and β_1(grey) with fibronectin 9^{th} and 10^{th} domains(purple) with RGD ligand(green). Blue spots represent ion-binding sites, and red and yellow structures are carbohydrate moieties used for protein crystallisation. Modified from M.Nagae (2012) [33].

Another hypothesis could be that integrin is promiscuous and the alginate chain can bind to the integrin un-specifically. F.Fogerty et al. (1990) hypothesised that integrins bind to the non-RGD part of fibronectin [97]. E.Koivunen (1994) found that integrin binds other sequences such as SDV(Ser-Asp-Val), SFT (Ser-Phe-Thr) and RNS (Arg-Asn-Ser), which are found on the fibronectin structure [88]. Such RGD-independent interaction between $\alpha_5\beta_1$ integrins and collagen has been identified [98].

The last hypothesis is that RGD-containing peptide requires the RGD to be embedded within the fibronectin protein in order to bind $\alpha_5\beta_1$ integrins efficiently, as synergy site found on fibronectin enhance the interaction. Studies have shown that the binding between integrin $\alpha_5\beta_1$ and fibronectin involves more than just an RGD-binding site. Two sites are involved in integrin and fibronectin binding: RGD, which is located in the 10th type III repeat (FN III10) that binds to the grove between the two subunits, and the "synergy sequence" (PHSRN : Pro-His-Ser-Arg-Asn) in the 9th type III repeat

(FN III9) that has contact with α_5 [99]. The synergy site showed a great enhancement effect on the biding of $\alpha_5\beta_1$ by facilitating the initial encounter of proteins, although it had little effect on the stability of the complex [92]. T.Petrie et al. (2006) demonstrated significantly increased adhesion strength by incorporating RGD within recombinant fibronectin structures compared to free peptide fragments [100].

Therefore, reduced affinity is expected from the RGDs grafted on alginate compared to the RGD within fibronectin. In single molecular spectrometry, low concentration of substrates and short interaction time is used in order to ensure single molecular interactions. However, such interaction force can be very difficult to measure when the ligand affinity is so low. Reason for this may be that, the interaction cannot be achieved at all during the given time, the interaction has shorter lifetime than the measurement time-span, or even if the interaction is achieved, the force jumps obtained can be masked by other noise.

This argument can be supported by a series of papers that have measured single molecular binding between RGD and Integrin $\alpha_5\beta_1$ (Table 4), using fibronectin as a ligand, rather than peptide.

Table 4. References of dynamic force spectroscopy measurements for integrins and RGD-peptides

Integrin	RGD	Reference
Purified human $\alpha_5\beta_1$ on tip	GRGDSP and PHSRN containing peptide amphiphile on surface	E. Kokkoli, 2005 [101]
$\alpha_5\beta_1$ expressing K562 on tip	Human plasma fibronectin on surface	F. Li, 2003 [102]
$\alpha_5\beta_1$ embedded in supported lipid bilayer on surface	Fibronectin on tip	D. Nordin,2012 [69]
Vascular smooth muscle cell on surface	Fibronectin or collagen coated bead on tip	Z. Sun, 2012 [103]
Antibody immobilised recombinant $\alpha_5\beta_1$ fused with Fc domain on surface with anti-Fc protein	Fibronectin on tip	F. Kong, 2009 [79]
$\alpha_5\beta_1$ or $\alpha_v\beta_1$ expressing osteoblasts	GRGDSP, GRGESP and GRADSP peptides on PEG coated tip.	P.P.Lehenkari, 1999 [104]
$\alpha_{IIb}\beta_3$ on platelet	Synthetic peptide (GSSSGRGDSPA) on the tip	I. Lee, 2001 [105]

5.6 Interaction measured between POA-GRGDYP and silane surface

No significant interaction between POA-GRGDYP and the silane surface was measured. However, it is important to mention such phenomenon, which will be discussed in this section. Non-specific interaction was expected between silane and the POA-GRGDYP tip, but as shown in Figure 5.12, higher magnitude of force jumps and higher frequency of taping reactions were observed. The following reasons may explain the interaction between the silane surface and the POA-GRGDYP tip.

The surface silane used (TETA) contains three carboxylic groups at the end of the molecules that were negatively charged at pH 7.4. R.Major and X.Zhu (2003) have showed Cu^{2+} chelating effect towards the carboxylic groups on 16-mercapto-hexadecanoic acid [106]. The same effect is expected for the manganese or magnesium cations, which have chelating effect on the carboxylic acid groups on the silane and alginate backbones. The same silane (TETA) used for surface immobilisation in this experiment has been shown to be efficient in heavy metal absorption, as described in Figure 5.17 [107].

In order to support the argument that cations in the buffer gives chelating effect between the carboxylic groups on the alginate and the carboxylic groups on the silane surface, the buffer was changed to MQ-water, and as the Figure 5.16 shows, almost no peeling reaction was observed while a very high frequency of large force jump reactions were observed.

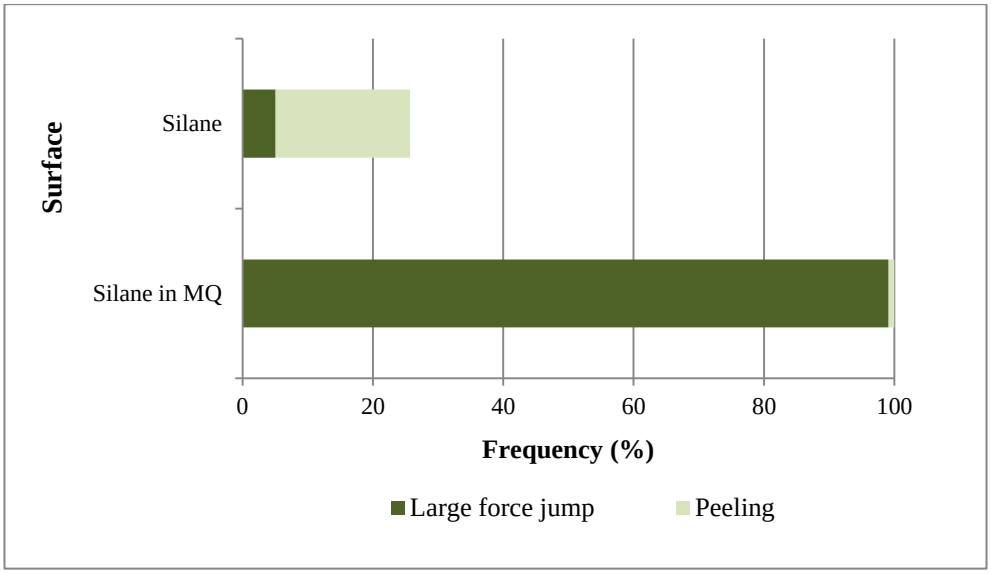

Figure 5.16. POA-GRGDYP tip and silane surface interaction
Peeling reaction disappears as the buffer was changed to MQ-water. (Standard deviation could not be calculated as the graph is based on one set of measurement. Based on the counting is provided in Appendix H)

As a conclusion, such metal chelating effect might have formed a series of adhesion interactions between alginate and silanes and caused peeling reaction to be observed. This can also be supported by the phenomenon that the peeling reaction is reduced or disappears when the surface was covered with other proteins (e.g. insulin and integrin, Figure 5.6 and Figure 5.8), or the buffer was changed to MQ-water (Figure 5.16).

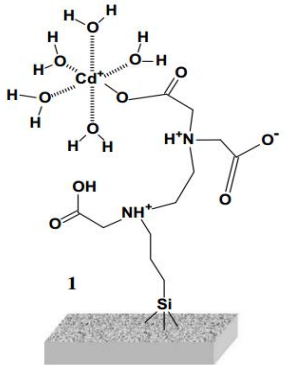

Figure 5.17. Chelating effect of heavy metal (Cd^{+}) on TETA immobilised on surface
Taken from A.Vasilieva et al. (2009) [107].

5.7 Advantage and disadvantages of AFM

It can be questioned whether using AFM was suitable or not at measuring the interaction. The main advantages of AFM for ligand-receptor system is that AFM allows measurement of single ligand-receptor interactions and characterisation of the activity of integrin under controlled force loads. However, the limitation is that such high sensitivity makes it difficult to discriminate between specific interactions from non-specific interactions [108]. In addition, the loading rate is significantly longer (2.0 nN/s) than the real physiological impulse time, which is near to zero [109].

6 Further studies

In order to achieve successful interactions between RGD-coupled alginate and $\alpha_5\beta_1$ integrin, factors prevented the molecules from interacting need to be identified. Either the system on the tip or the system on the surface could be modified.

Assuming that GRGFYP-POA could not interact with integrins, the tip could be immobilised with other ligands. For instance, fibronectin or RGD-peptides with a linker could be used. The use of fibronectin would be advantageous as it is the natural receptor for $\alpha_5\beta_1$ integrin, and it has previously been immobilised on the tip, achieving successful interactions [69, 79]. RGD-peptides could be linked with either PEG [104] or a series of small amino acid (such as Serine or Glycine) [105].

If the integrin surface was non-interactive with RGD-coupled alginate, changing the surface could result in successful interactions. As discussed in Result and Discussion 5.5, integrins could be embedded in SBL [69] or transmembrane-truncated integrins could be used. Capturing of integrins could be tried again with a different antibody.

.

7 Conclusion

Atomic force microscopy was used to investigate single-molecule interactions between RGD-coupled alginate and $\alpha_5\beta_1$ integrin.

At the early stage of the investigation, alginate was coupled with GRGDSP by a carbodiimide chemistry, obtaining 0.53% coupling. When the alg-GRGDSP and $\alpha_5\beta_1$ integrins were immobilised by the carbodiimide chemistry on silanised tip and silanised surface, respectively, the molecules did not show any significant number of interaction frequency.

Several modifications were attempted for improving the interactions between the peptide and the integrin. About 10 times more coupling was obtained (the first batch 4.8% and the second batch 5.5%) by coupling alginate to peptides by using periodate oxidation followed by the reductive amination method. For the surface, integrins were captured with antibodies to orientate the integrins into upright position. In order to measure specific interactions between POA-GRGDYP, four different surfaces were tested : 1) Integrin captured by antibody surface, 2) Integrin (captured by antibody) that were blocked by solubilised GRGDYP peptides, 3) Antibody surface and 4) Silane surface. No specific interaction was achieved, since similar interaction frequencies and profiles were observed for the integrin surface and the blocked integrin surface. The antibody surface showed slightly higher magnitude of rupture force, while the silane surface showed a much higher magnitude of rupture force

In addition, insulin surface was tested as a blocking material in order to reduce the high interaction noise caused by the silane surface, however insulin showed interactivity as high as integrin.

In order to investigate the high adhesion phenomenon found for silane tip and silane surface, the interaction between the silane surface and silane tip was also investigated. Interestingly, a high rate of peeling reactions was observed.

Knowing the interaction profiles between RGD-alginate and integrins, the efficiency and potential influence of RGD-coupled alginate as a biomaterial could be further investigated. Although the interaction was not characterised in this study, the presented result may aid future investigations on the same system.

Bibliography

1. Ratner, B.D. and S.J. Bryant, *BIOMATERIALS: Where We Have Been and WhereWe Are Going.* Annual Review of Biomedical Engineering, 2004. 6: p. 41.
2. Williams, D.F., *On the mechanisms of biocompatibility.* Biomaterials, 2008. 29(20): p. 2941-53.
3. Melvik, J.E. and M. Dornish, *Alginate as a Carrier for Cell Immobilisation.* Fundamentals of Cell Immobilisation Biotechnology, 2004. 8A: p. 33-51.
4. Ruoslahti, E., *RGD and other recognition sequences for integrins.* Annual review of cell and developmental biology, 1996. 12: p. 697-715.
5. Stanford, E.C.C., B. patent, Editor. 1881.
6. Smidsrød, O. and A. Haug, *selectivity of some anionic polymers for divalent metal ions.* acta chemica scandinavica, 1970. 24: p. 843-54.
7. T., H., et al., *Food Stabilisers, Thickeners and Gelling Agents*, ed. A. Imeson. 2010: Blackwell Publishing Ltd.
8. Cimini, D., M.D. Rosa, and C. Schiraldi, *Production of glucuronic acid-based polysaccharides by microbial fermentation for biomedical applications.* Biotechnology journal, 2012. 7(2): p. 237-50.
9. Draget, K.I., G. Skjåk-Bræk, and O. Smidsrød, *Alginate based new materials.* International Journal of Biological Macromolecules, 1997. 21: p. 47-55.
10. Tøndervik, A., et al., *Mannuronan C-5 epimerases suited for tailoring of specific alginate structures obtained by high-throughput screening of an epimerase mutant library.* Biomacromolecules, 2013. 14(8): p. 2657-66.
11. Ertesvåg, H., et al., *Mannuronan C-5-Epimerases and Their Application for in Vitro and in Vivo Design of New Alginates Useful in Biotechnology.* Journal of Metabolic Engineering, 1999. 1: p. 262-69.
12. Sabra, W. and A.P. Zeng, *Microbial Production of Alginates: Physiology and Process Aspects* in *Alginates: Biology and Applications*, B.H.A. Rehm, Editor. 2009, Springer. p. 154-168.
13. Sikorski, P., et al., *Evidence for Egg-Box-Compatible Interactions in Calcium-Alginate Gels from Fiber X-ray Diffraction.* Biomacromolecules, 2007. 8(7): p. 2098-203.
14. Donati, I., et al., *New Hypothesis on the Role of Alternating Sequences in Calcium-Alginate Gels.* Biomacromolecules, 2005. 6: p. 1031-40.
15. Stokke, B.T., et al., *Small-Angle X-ray Scattering and Rheological Characterization of Alginate Gels . 1 . Ca - Alginate Gels.* Macromolecules, 2000. 33: p. 1853-63.
16. Gombotz, W.R. and S.F. Wee, *Protein release from alginate matrices.* Advanced Drug Delievery, 1998. 31: p. 267-85.
17. Smetana, K., *Cell biology of hydrogels* Biomaterials, 1993. 14(14): p. 1046-51.
18. Augst, A.D., H.J. Kong, and D.J. Mooney, *Alginate Hydrogels as Biomaterials.* Macromolecular Bioscience, 2006. 6(8): p. 623-33.
19. Ludwig, B., et al., *A novel device for islet transplantation providing immune protection and oxygen supply.* Hormone and Metabolism Research, 2010. 42(13): p. 918-922.

20. Dufrane, D., et al., *Six-month survival of microencapsulated pig islets and alginate biocompatibility in primates: proof of concept.* Transplantation, 2006. 81(9): p. 8.
21. Poojari, R. and R. Srivastava, *Composite alginate microspheres as the next-generation egg-box carriers for biomacromolecules delivery.* Expert opinion on drug delivery, 2013. 10(8): p. 1061-76.
22. Bidarra, S.J., C.C. Barrias, and P.L. Granja, *Injectable alginate hydrogels for cell delivery in tissue engineering.* Acta Biomaterialia, 2014: p. 1742-61.
23. Lee, S.-J. and A. Atala, *Scaffold technologies for controlling cell behavior in tissue engineering.* 2013. 8: p. 10201-3.
24. Rowley, J., G. Madlambayan, and D. Mooney, *Alginate hydrogels as synthetic extracellular matrix materials.* Biomaterials, 1999. 20: p. 45-53.
25. Hynes, R.O., *Integrins: versatility, modulation, and signaling in cell adhesion.* Cell, 1992. 69: p. 11-25.
26. Hynes, R.O., *Integrins : Bidirectional , Allosteric Signaling Machines* Cell, 2002. 110: p. 673-87.
27. Hynes, R.O., *Integrins: A Family of Cell Curface Receptors.* Cell, 1987. 45: p. 549-54.
28. Barczyk, M., S. Carracedo, and D. Gullberg, *Integrins.* Cell Tissue Res, 2010. 339: p. 269-80.
29. Medicine, U.S.N.L.o. *Integrin alpha5beta1*. MeSH Descriptor Data 2011 31 August 2011 [cited 2014 04 May]; Available from: http://www.nlm.nih.gov/cgi/mesh/2011/MB_cgi?mode=&term=Integrin+alpha5beta1&field=entry.
30. Francis, S.E., et al., *Central Roles of alpha5beta1 Integrin and Fibronectin in Vascular Development in Mouse Embryos and Embryoid Bodies.* Arteriosclerosis, Thrombosis, and Vascular Biology, 2002. 22(6): p. 927-33.
31. Pimton, P., et al., *Fibronectin-mediated upregulation of α5β1 integrin and cell adhesion during differentiation of mouse embryonic stem cells.* Cell Adhesion & Migration, 2011. 5: p. 73-82.
32. Jeschke, B., et al., *RGD-peptides for tissue engineering of articular cartilage.* Biomaterials, 2002. 23(16): p. 3455-63.
33. Nagae, M., et al., *Crystal structure of alpha5 beta1 integrin ectodomain: Atomic details of the fibronectin receptor.* The Journal of cell biology, 2012. 197(1): p. 131-40.
34. Delannet, M., et al., *Specific roles of the alpha V beta 1, alpha V beta 3 and alpha V beta 5 integrins in avian neural crest cell adhesion and migration on vitronectin.* Development, 1994. 120: p. 2687-92.
35. Zhang, K. and J. Chen, *The regulation of integrin function by divalent cations* Cell Adhesion & Migration, 2012. 6(1): p. 20-9.
36. Campbell, I.D. and M.J. Humphries, *Integrin Structure, Activation, and Interactions.* Cold Spring Harb Perspect Biol, 2011. 3(3): p. 1-15.
37. Mould, A.P., S.K. Akiyama, and M.J. Humphries, *Regulation of Integrin alpha5beta1-Fibronectin Interactions by Divalent Cations.* Journal of Biololgical Chemistry, 1995. 270(44): p. 26270-7.
38. Tiwari, S., et al., *Divalent cations regulate the folding and activation status of integrins during their intracellular trafficking.* Journal of Cell Science, 2011. 124: p. 1672-80.

39. Takagi, J. and T.A. Springer, *Integrin activation and structural rearrangement.* Immunological Reviews, 2002. 186: p. 141-63.
40. Beer, J.H., K.T. Springer, and B.S. Coller, *Immobilized Arg-Gly-Asp (RGD) peptides of varying lengths as structural probes of the platelet glycoprotein IIb/IIIa receptor.* blood, 1992. 79: p. 117-28.
41. Bouhadir, K.H., et al., *Polymers containing polysaccharides such as alginates or modified alginates*. 1998.
42. McDonagh, B.H., *Optimalised Carbodiimide Chemistry for RGD-coupled Alginate*, in *Biotechnology*. 2012, NTNU: Trondheim.
43. Gomez, C.G., M. Rinaudo, and M.A. Villar, *Oxidation of sodium alginate and characterization of the oxidized derivatives.* Carbohydrate Polymers, 2007. 67: p. 296-304.
44. Vold, I.M., K.A. Kristiansen, and B.E. Christensen, *A study of the chain stiffness and extension of alginates, in vitro epimerized alginates, and periodate-oxidized alginates using size-exclusion chromatography combined with light scattering and viscosity detectors.* Biomacromolecules, 2006. 7(7): p. 2136-46.
45. Bouhadira, K.H., D.S. Hausmana, and D.J. Mooney, *Synthesis of cross-linked poly(aldehyde guluronate) hydrogels.* Polymer, 1999. 40: p. 3575-84.
46. Painter, T. and B. Larsen, *Formation of Hemiacetals between neighbouring hexuronic acid residues during the periodate oxidation of alginate.* Acta chemica scandinavica, 1970. 24: p. 813-33.
47. Ruhaak, L.R., et al., *2-Picoline-Borane: a Non-Toxic Reducing Agent for Oligosaccharide Labeling By Reductive Amination.* Proteomics, 2010. 10(12): p. 6.
48. Kristiansen, K.A., et al., *An evaluation of tritium and fluorescence labelling combined with multi-detector SEC for the detection of carbonyl groups in polysaccharides.* Carbohydrate Polymers, 2009. 76(2): p. 196-205.
49. Kristiansen, K.A., et al., *Novel alginates prepared by independent control of chain stiffness and distribution of G-residues: Structure and gelling properties.* Carbohydrate Polymers, 2009. 77(4): p. 725-35.
50. Bouhadir, K.H., et al., *Degradation of partially oxidized alginate and its potential application for tissue engineering.* Biotechnology progress, 2001. 17(5): p. 945-50.
51. Al-Shamkhani, A. and R. Duncan, *Radioiodination of alginate via covalently-bound tyrosinamide allows monitoring of its fate in vivo.* Journal of Bioactive and Compatible Polymers, 1995. 10: p. 4.
52. Gao, C., et al., *Preparation and controlled degradation of oxidized sodium alginate hydrogel.* Polymer Degradation and Stability, 2009. 94: p. 1405-1410.
53. Binnig, G., C.F. Quate, and C. Gerber, *Atomic Force Microscope.* Physical Review Letters, 1986. 56(9): p. 3.
54. Sletmoen, M., et al., *Single-Molecule Pair Studies of the Interactions of the a-GalNAc (Tn-Antigen) Form of Porcine Submaxillary Mucin With Soybean Agglutinin.* Biopolymers, 2009. 91(9): p. 719-728.
55. Gomez-Casado, A., et al., *Charge-Transfer Complexes Studied by Dynamic Force Spectroscopy.* Journal of Polymers, 2013. 5(1): p. 269-83.
56. Albrecht, T.R., et al., *Microfabrication of cantilever styli for the atomic force microscope.* Journal of Vacuum Science & Technology, 1990. 8: p. 3386-96.
57. Tortonese, M., *Cantilevers And Tips For Atomic Force Microscopy* IEEE Engineering in Medicine and Biology Magazine, 1997(March/April): p. 28-33.

58. Cumpson, P.J., et al., *chapter8. Cantilever Spring-Constant Calibration in Atomic Force Microscopy*. 2008. 25.
59. Slattery, A.D., et al., *Accurate measurement of Atomic Force Microscope cantilever deflection excluding tip-surface contact with application to force calibration.* Ultramicroscopy, 2013. 131: p. 46-55.
60. Hutter, J.L. and J. Bechhoefer, *Calibration of atomic-force microscope tips.* Review of Scientific Instruments, 1993. 64(7): p. 1868-73.
61. Hutter, J.L. and J. Bechhoefer. *Calibration of AFM Cantilevers*. 2005 2005 [cited 2014 5.May]; Available from: http://www.physics.uwo.ca/~hutter/calibration/afmcal.html.
62. Munoz, V., et al., *Folding dynamics and mechanism of beta-hairpin formation.* Nature, 1997. 390: p. 196-9.
63. Håti, A.G., *Single molecule dynamic force spectroscopy of alginate-mannuronan C-5 epimerase interactions using optical tweezers*, in *Biophysics and medical technology*. 2012, NTNU: Trondheim.
64. Evans, E. and K. Ritchie, *Dynamic Strength of Molecular Adhesion Bonds.* Biophysical Journal, 1997. 72: p. 1541-5.
65. Evans, E., *Energy landscapes of biomolecular adhesion and receptor anchoring at interfaces explored with dynamic force spectroscopy.* Faraday discussions, 1998. 111: p. 1-16.
66. Evans, E., *Looking inside molecular bonds at biological interfaces with dynamic force spectroscopy.* Biophysical chemistry, 1999. 82: p. 83-97.
67. Sletmoen, M., G. Skjåk-Bræk, and B.T. Stokke, *Single-molecular Pair Unbinding Studies of Mannuronan C-5 Epimerase AlgE4 and Its Polymer Substrate.* Biomacromolecules, 2004. 5: p. 1288-95.
68. Humphries, M.J., et al., *Integrin structure: heady advances in ligand binding, but activation still makes the knees wobble.* Trends in Biochemical Sciences, 2003. 28(6): p. 313-320.
69. Nordin, D., L. Donlon, and D. Frankel, *Characterising single fibronectin-integrin complexes.* Soft Matter, 2012. 8: p. 6151-60.
70. Fjelldal, M.F., *Study of Rat Olfactory Ensheathing Cells in Alginate based Matrices*, in *Department of Biotechnology*. 2012, Norwegian University of Science and Technology. p. 127.
71. Kristiansen, K.A., A. Potthast, and B.E. Christensen, *Periodate oxidation of polysaccharides for modification of chemical and physical properties.* Carbohydrate Research, 2010(345): p. 1264-71.
72. Fadeev, A.Y. and T.J. McCarthy, *Self-Assembly Is Not the Only Reaction Possible between Alkyltrichlorosilanes and Surfaces: Monomolecular and Oligomeric Covalently Attached Layers of Dichloro- and Trichloroalkylsilanes on Silicon.* Langmuir, 2000. 16: p. 7268-74.
73. Baumgärtel, T., C. Borczyskowski, and H. Graaf, *Selective surface modification of lithographic silicon oxide nanostructures by organofunctional silanes.* Beilstein journal of nanotechnology, 2013. 4: p. 218-26.
74. Vallant, T., et al., *Formation of Self-Assembled Octadecylsiloxane Monolayers on Mica and Silicon Surfaces Studied by Atomic Force Microscopy and Infrared Spectroscopy.* Journal of Physical Chemistry, 1998. 5647(98): p. 7190-7.
75. Arkles, B., *Silane Coupling Agents, Connecting Across Boundaries v2.0*, I. Gelest, Editor. 2006. p. 57-60.

76. Lill, K.J., *Alginat - protein interaksjoner*, in *Biotechnology*. 2011, NTNU: Trondheim.
77. Ratcliff, G.C. and D.A. Erie, *A Novel Single-Molecule Study To Determine Protein-Protein Association Constants.* Journal of American Chemistry, 2001. 123: p. 5632-5.
78. Harada, Y., M. Kuroda, and A. Ishida, *Specific and Quantized Antigen-Antibody Interaction Measured by Atomic Force Microscopy.* Langmuir, 1999. 16: p. 708-715.
79. Kong, F., et al., *Demonstration of catch bonds between an integrin and its ligand.* The Journal of Cell Biology, 2009. 185(7): p. 9.
80. Takagi, J., *Molecular Environment of Integrins Molecular Environment of Integrins.* Biochemical Society Transaction, 2004. 32: p. 403-6.
81. Sainchez-Aparicio, P., C. Dominguez-Jimenez, and A. Garcia-Pardo, *Activation of the tx4/31 Integrin through the/31 Subunit Induces Recognition of the RGDS Sequence in Fibronectin.* The Journal of Cell Biology, 1994. 126(1): p. 271-9.
82. Biolegend. *Purified anti-human CD29 Antibody*. 2012 [cited 2013 13. May]; Available from: http://www.biolegend.com/purified-anti-human-cd29-antibody-855.html.
83. Zlatanovaa, J., S.M. Lindsay, and S.H. Leuba, *Single molecule force spectroscopy in biology using the atomic force microscope.* Progress in Biophysics & Molecular Biology, 2000. 74: p. 37-61.
84. Holmberg, A., et al., *The biotin-streptavidin interaction can be reversibly broken using water at elevated temperatures.* Electrophoresis, 2005. 26: p. 501-10.
85. Pierce, M.M., C.S. Raman, and B.T. Nall, *Isothermal Titration Calorimetry of Protein Protein Interactions.* Methods, 1999. 19: p. 213-21.
86. Karstensen, K., *Novel alginate matrix for tissue engineering: selective substitution ofmannuronic acid residues in alginate with bioactive peptides and the use of these polymers as scaffolds for cells*, in *Department of Biotechnology*. 2010, NTNU: Trondheim.
87. Hersel, U., C. Dahmen, and H. Kessler, *RGD modified polymers: biomaterials for stimulated cell adhesion and beyond.* Biomaterials, 2003. 24: p. 4385-415.
88. Koivunen, E., B. Wang, and E. Ruoslahti, *Isolation of a highly specific ligand for the alpha 5 beta 1 integrin from a phage display library.* The Journal of cell biology, 1994. 124(3): p. 373-80.
89. Scolastico, C. and G. Giannini, *Peptido-mimetic compounds containing RGD sequence useful as integrin inhibitors*. 2001: US.
90. Mardilovich, A. and E. Kokkoli, *Biomimetic peptide-amphiphiles for functional biomaterials: the role of GRGDSP and PHSRN.* Biomacromolecules, 2004. 5(3): p. 950-7.
91. Hemler, M.E., et al., *Structure, biochemical properties, and biological functions of integrin cytoplasmic domains*. Integrins: The biological problems, ed. TakadaY. 1995: CRC Press. 35.
92. Takagi, J., et al., *Structure of integrin alpha5beta1 in complex with fibronectin.* The EMBO journal, 2003. 22(18): p. 4607-15.
93. Coe, A.P.F., et al., *Generation of a Minimal alpha-5 beta-1 Integrin-Fc Fragment.* Journal of Biololgical Chemistry, 2001. 276: p. 35854-35866.

94. Greenberg, Z., et al., *Covalent Immobilization of Recombinant Human alpha v beta 3 Integrin on a Solid Support with Retention of Functionality.* Analytical Biochemistry, 1999. 266: p. 153-64.
95. Janshoff, A., et al., *Force Spectroscopy of Molecular Systems-Single Molecule Spectroscopy of Polymers and Biomolecules.* Angewandte Chemie (International ed. in English), 2000. 39(18): p. 3212-37.
96. Lee, P.M., K.H. Lee, and Y.S. Siaw, *Covalent immobilization of aminoacylase to alginate for L-phenylalanine production.* Journal of chemical technology and biotechnology, 1993. 58(1): p. 65-70.
97. Fogerty, F.J., et al., *Inhibition of Binding of Fibronectin to Matrix Assembly Sites by Anti-Integrin Antibodies.* The Journal of Cell Biology, 1990. 111: p. 699-708.
98. Kramer, R.H. and N. Marks, *Identification of integrin collagen receptors on human melanoma cells.* The Journal of biological chemistry, 1989. 264: p. 4684-8.
99. Danen, E.H.J., et al., *Requirement for the Synergy Site for Cell Adhesion to Fibronectin Depends on the Activation State of Integrin α5β1.* Journal of Biololgical Chemistry, 1995. 270: p. 21612-8.
100. Petriea, T.A., et al., *Integrin specificity and enhanced cellular activities associated with surfaces presenting a recombinant fibronectin fragment compared to RGD supports.* Biomaterials, 2006. 27: p. 5459-70.
101. Kokkoli, E. and A. Mardilovich, *The Use of Atomic Force Microscopy a5b1 in Characterizing Ligand-Receptor (α β Integrin) Interactions*, in *In Applications of Scanned Probe Microscopy to Polymers*, J. Batteas, et al, Editor. 2005, American Chemical Society. p. 182-192.
102. Li, F., et al., *Force Measurements of the a5b1 Integrin–Fibronectin Interaction.* Biophysical Journal, 2003: p. 1252-62.
103. Sun, Z., Z. Li, and G.A. Meininger, *Mechanotransduction through fibronectin-integrin focal adhesion in microvascular smooth muscle cells: is calcium essential?* American Journal of Heart and Circulatory Physiology 2012. 302: p. 1965-73.
104. Lehenkari, P.P. and M.A. Horton, *Single integrin molecule adhesion forces in intact cells measured by atomic force microscopy.* Biochemical and Biophysical Research Communications, 1999. 259(3): p. 645-50.
105. Lee, I. and R.E. Marchant, *Force measurements on the molecular interactions between ligand (RGD) and human platelet αIIbβ3 receptor system.* Surface Science, 2001. 491(3): p. 433-43.
106. Major, R.C. and X.Y. Zhu, *The Surface Chelate Effect.* JACS communication, 2003. 125(28): p. 8454-6.
107. Vasilieva, A.N., et al., *Adsorption of heavy metal cations by organic ligands grafted on porous materials.* Microporous and Mesoporous Materials, 2009. 118: p. 251-7.
108. Neuman, K.C. and A. Nagy, *Single-molecule force spectroscopy: optical tweezers, magnetic tweezers and atomic force microscopy.* Nature Methods, 2012. 5(6): p. 491-505.
109. Ando, T., et al., *A high-speed atomic force microscope for studying biological macromolecules.* Proceedings of National Academic of Science, 2001. 98(22): p. 12468-72.

Appendices

Appendix A. Analysis of GRGDSP-coupled alginate

RESEARCH USE

FMC BioPolymer AS
d/b/a NovaMatrix

COMMONWEALTH BIOTECHNOLOGIES, INC.

601 Biotech Dr., Richmond, VA 23235
phone: 800-725-9225
phone: 804-648-3820
fax: 804-648-2641
www.cbi-biotech.com
email: info@cbi-biotech.com

CERTIFICATE OF ANALYSIS
FMC RAUH 02 (Gly-Arg-Gly-Asp-Ser-Pro)– Alginate Complex

Lot number: CBIFMC02A04112907
Production Date: 11/29/07

13.1 grams

The characteristics of the peptide-alginate complex are as follows:

1. **APPEARANCE:** white lyophilate
2. **PEPTIDE CONTENT**
   by Amino Acid Analysis (CBI SOP AMACANAL0002): 0.0269 µmol per mg solid
3. **ALGINATE CONTENT**
   by calculation: 0.0044 µmol per mg solid
4. **PEPTIDE: ALGINATE RATIO:** 6.11:1 by amino acid analysis)
5. **SOLUBILITY:** soluble in water to < 2% (w/v)
6. **ENDOTOXIN CONTENT** (CBI SOP GENPROC0009) 0.02 EU per mg
7. **AMINO ACID ANALYSIS**

Residue	Residues per mol			Residue	Residues per mol		
	Observed	Integer	Theor		Observed	Integer	Theor
As(x)	1.28	1	1	Val	0	0	--
Gl(x)	0	0	--	Met	0	0	--
Ser	1.03	1	1	Trp	Not Determined		
His	0	0	--	Phe	0	0	--
Gly	2.29	2	2	Ile	0	0	---
Thr	0	0	--	Leu	0	0	--
Ala	0	0	--	Lys	0	0	--
Arg	1.19	1	1	Pro	0.78	1	1
Tyr	0	0	--	Cys	Not Determined		
Cystine	Not Determined						

Tammie Crabtree — 11/29/07

Name: Tammie Crabtree
Laboratory Manager, CBI

Date

A-Figure 1. Analysis sheet of GRGDSP-coupled alginate purchased from FMC Biopolymer

Calculations of degree of peptide substitution

Number of alginate monomers per mg (Assuming all sample is alginate),

- Number of alginate monomers per mg (assuming all the contents is alginate) = $\frac{1mg}{198\ \text{mg/mmol}}$ = 0.00505 mmol/mg = 5.05μmol/mg

As the alginate contents is given as 0.0044 μmol/mg solid

- DP_n (Degree of Polymerisation) is defined as the number of monomer units in a polymer chain = $\frac{number\ of\ monomers\ per\ 1mg}{number\ of\ chains\ per\ 1mg}$ = $\frac{5.05\ \mu\text{mol/mg}}{0.0044\ \mu\text{mol/mg}}$ = 1148 molecules per a alginate chain

Given peptide contents : 0.0269 μmol/mg

Two assumptions are made; alginate is 1mg (as the amount of peptide is relatively small) and number of carboxylic groups is same as the number of monomers (as one monomer contains one carboxylic group)

- % of substitution = $100 \times \frac{\text{peptide molecules}}{\text{Alginate monomers}}$ = $100 \times \frac{0.0269\ \mu\text{mol}}{5.05\ \mu\text{mol}}$ = 0.53%

* However NMR analysis of the sample (The graph is not provided) has given around 0.2~3% of substitution by H^1-NMR. Therefore, some percentage of the peptide is suspected not to be cross-linked to the alginate.

Appendix B. H^1-NMR spectra and analysis for POA-GRGDYP

Analysed by Marianne Ø knes Dalheim

Batch no. 1
Coupling reaction
december 2013
NMR 300 mhz
By: Marianne
File: 131209-3
Title: POA8%-
GRGDYP Hye Won

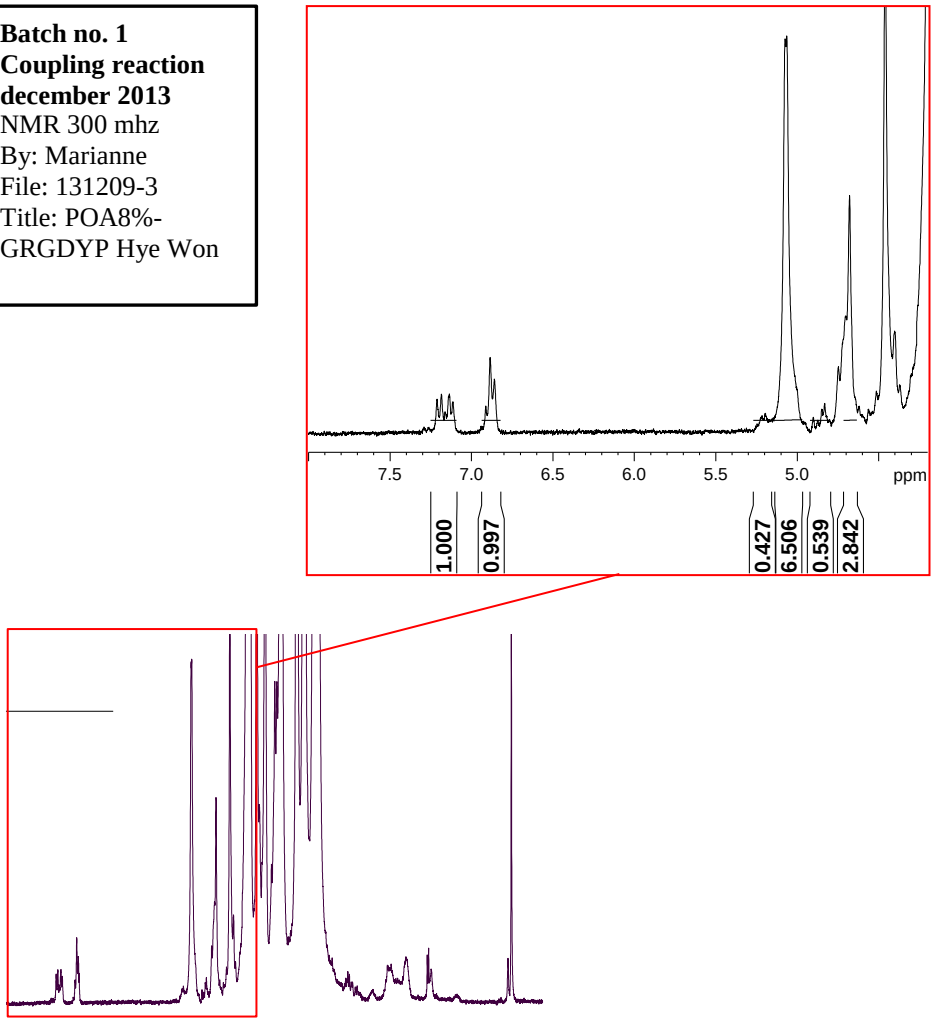

A-Figure 2. H^1-NMR spectrum for POA-GRGDYP batch 1

$$\textit{Degree of substitution} = \frac{I_{MeOTyr}}{4(I_{red\alpha} + I_{G-1} + I_{red\beta} + I_{M-1} + I_{MG-1})}$$

$$= \frac{1,000 + 0,997}{4(0,427 + 6,506 + 0,539 + 2,842)} \approx 4,8\%$$

Batch no.2
Coupling reaction
april 2014
NMR 300 mhz
By: Marianne
File: 140411-1
Title: POA-RGD tilsatt
8 µl TTHA (HWL)

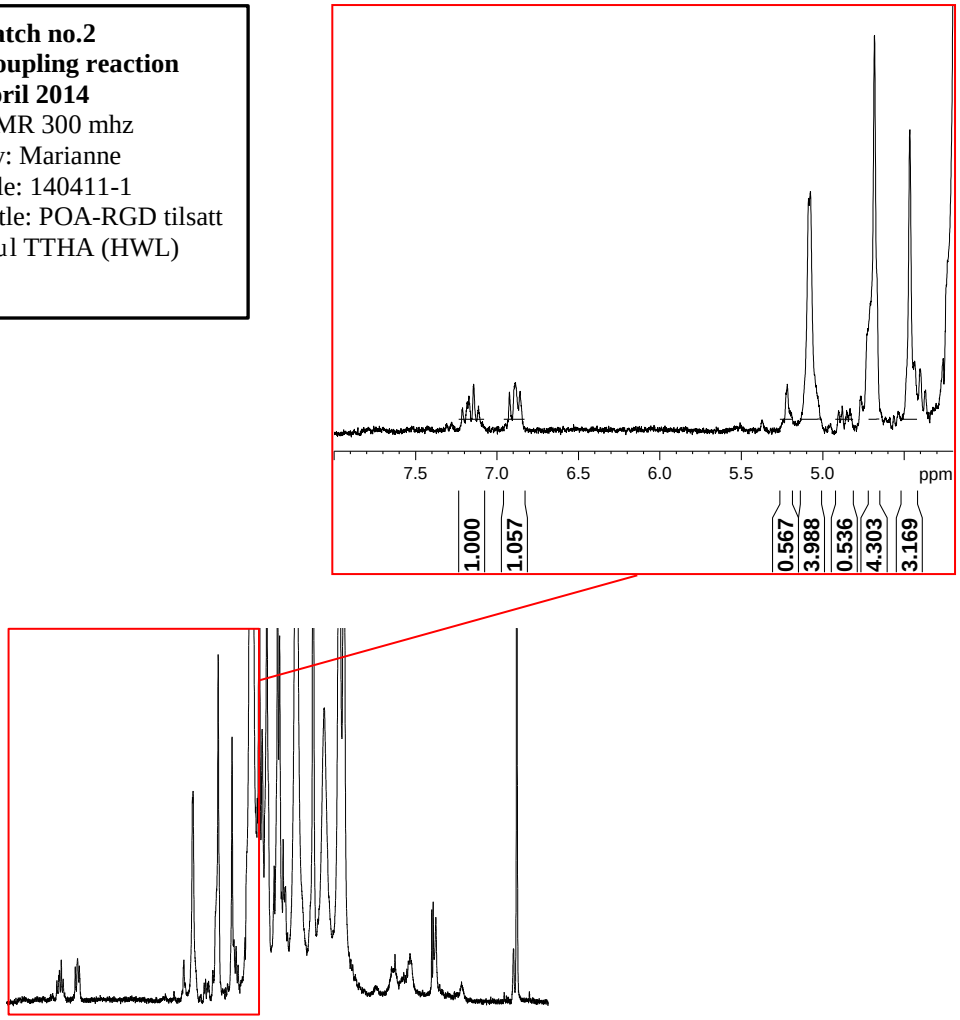

A-Figure 3. H[1]-NMR spectrum for POA-GRGDYP batch 2

$$\boldsymbol{Degree\ of\ substitution} = \frac{\boldsymbol{I_{Tyr}}}{\boldsymbol{4(I_{red\alpha} + I_{G-1} + I_{red\beta} + I_{M-1} + I_{MG-1})}}$$

$$= \frac{\boldsymbol{1,000 + 1.057}}{\boldsymbol{4(0.567 + 3.998 + 0.536 + 4.303)}} \approx \boldsymbol{5.5\%}$$

A-Table 1. Properties of the alginate (before periodate oxidation and GRGDYP coupling)

Batch no.	Alginate name	F_G	G_M	F_{GG}	F_{GM}	F_{MM}	F_{GGM}	F_{MGM}	F_{GGG}	$N_G>1$	[η] (ml/g)	$\sim M_w$ (g/mol)	$\sim M_n$ (g/mol)
1	LF10/60 (S22039)	0.68	0.32	0.57	0.11	0.21	0.042	0.079	0.53	14	530	103300	52600
2	HF120RB (S21967)	0.48	0.52	0.32	0.16	0.37	0.040	0.13	0.28	9	1125	271000	152600

- **Calculation for DP**

Batch no. 1 :

DP (LF10/60) = $\frac{M_n}{n} = \frac{52600\ g/mol}{198\ g/mol}$ = 265.7 monomers / chain

Average number of peptides per chain : $265.7 \times \frac{4.8}{100}$ = 12.8 peptides per chain

Batch no. 2 :

DP (HF120RB) = $\frac{M_n}{n} = \frac{152600\ g/mol}{198\ g/mol}$ = 770.7 monomers / chain

Average number of peptides per chain : $770.7 \times \frac{5.5}{100}$ = 42.4 peptides per chain

Appendix C. Base of frequency count for Figure 5.1

A-Table 2. Count of jumps for Figure 5.1

File name	Force jump*	percentage(%)
calibration	0/200	0
integrinSurface_2%Alginate	7/250	2.8
integrinSurface_2%Alginate(Speed1.0_Delay0.8)	3/151	1.9
integrinSurface_2%Alginate(Speed1.0_Delay1.2)	1/32	3.1
integrinSurface_2%Alginate(Speed2.0_Delay0.8)	3/42	7.1
integrinSurface_4% Alginate(Speed2.0_)	2/65	3.1
integrinSurface_4% Alginate(Speed2.0_Delay0.5)	5/250	2.0
integrinSurface_4% Alginate(Speed2.0_Delay1.0)	3/90	3.3
integrinSurface_4% Alginate(Speed2.0_Delay0.5)	0/40	0
silaneSurface_2% Alginate(Speed1.5_delay0.8)	0/140	0
Average	23/1060	2.3%
Standard deviation		2.1

*number of curves with interaction/ total number of curves

Appendix D. Base of the frequency count for Figure 5.3

A-Table 3. Count of jumps for Figure 5.3

Surface	Tip	Peeling*	Force Jump*	Sum(%)
2% Silane	No silane	1/721	70/721	
		0.1%	9.7%	9.8
	10 mins	67/640	17/640	
		10.4%	2.7%	13.1
	30 mins	38/642	16/642	
		5.9%	2.5%	8.4
5% Silane	No silane	6/634	41/721	
		1.4%	5.7%	7.1
	10 mins	38/320	3/320	
		11.9%	1.0%	12.9
	30 mins	31/320	2/642	
		9.7%	0.3%	10.0

*(number of curves with interaction/ total number of curves)

Appendix E. Length analysis of silane-silane interaction

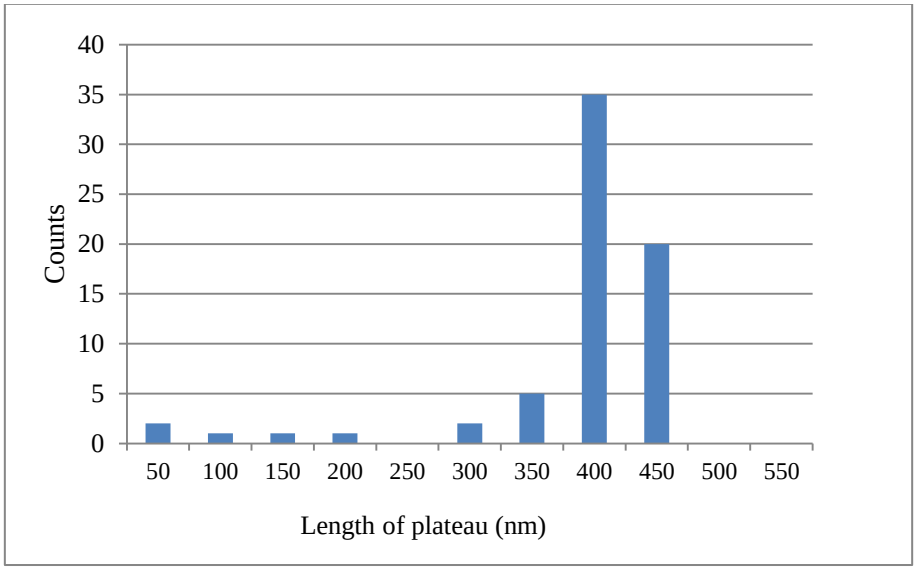

A-Figure 4. 2% (10mins) silane surface with (3%) 10mins silane tip

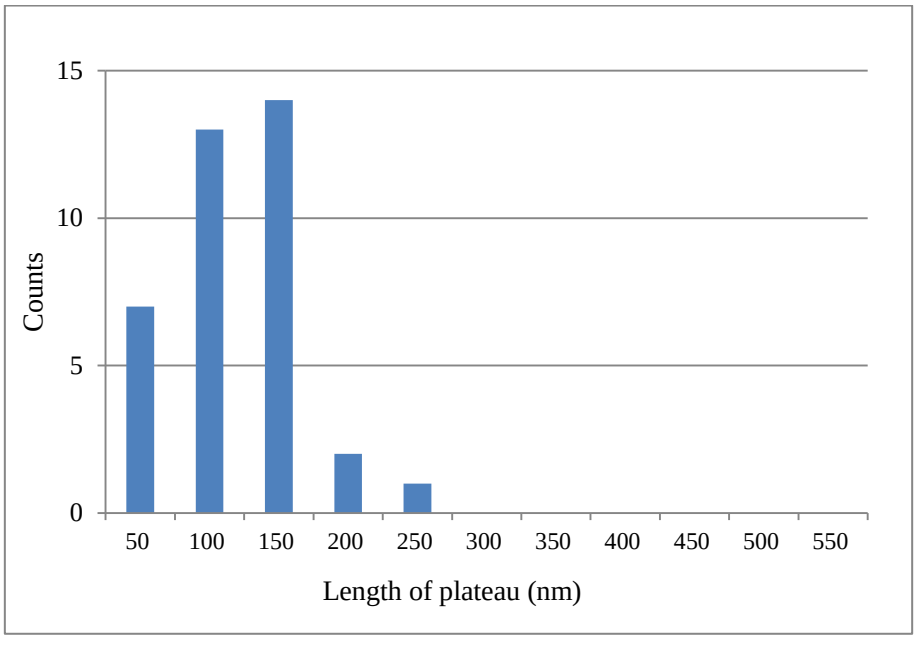

A-Figure 5. 2% (10mins) silane surface with (3%) 30mins silane tip

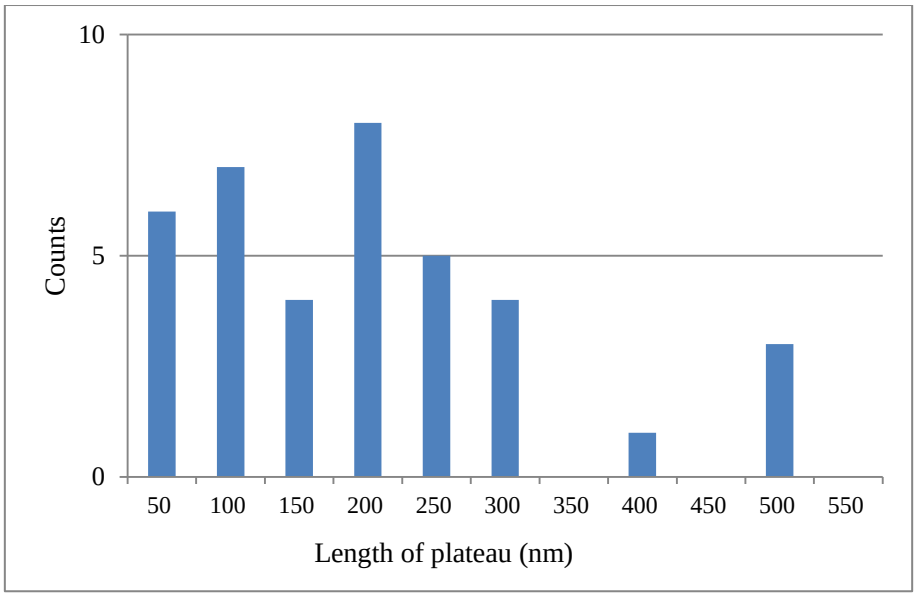

A-Figure 6. 5% (10mins) silane surface with (3%) 10mins silane tip

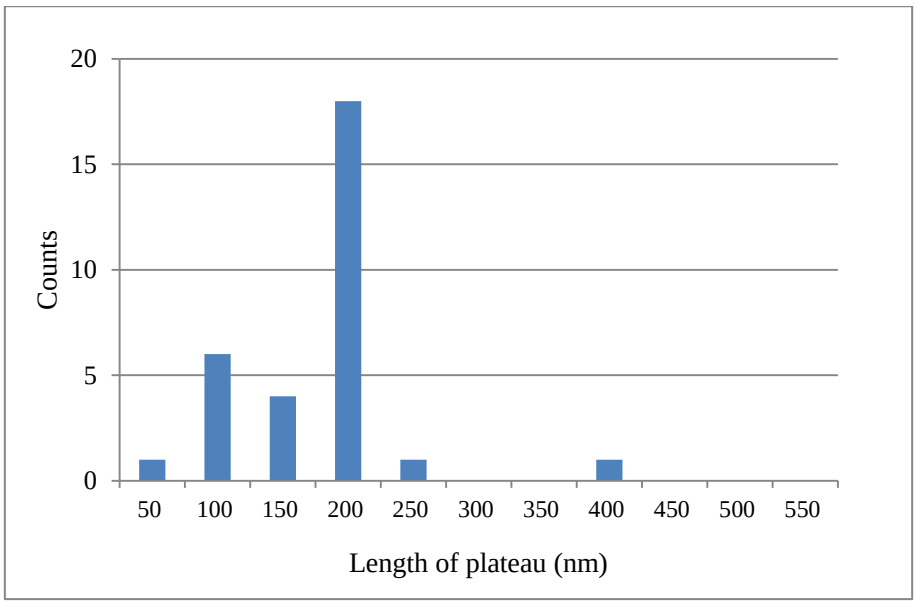

A-Figure 7. 5% (10mins) silane surface with (3%) 30mins silane tip

Appendix F. Base of the frequency count for Figure 5.6

A-Table 4. Count of jumps for Figure 5.6

Surface	Peeling*	Force Jump*	Sum(%)
mica			
Insulin	0/1125	173/1125	
	0%	15.3%	15.3
Integrin	74/1157	146/1157	
	6.4%	12.6%	19.0%

*(number of curves with interaction/ total number of curves)

Appendix G. Base of frequency count for Figure 5.8

A-Table 5. Count of jumps for Figure 5.8

Surface	Peeling*	Large*	Force Jump*	Sum(%)
Calibration	-	-	(1/100+4/327)+(0/200)	0.7
	-	-	0.7	
Integrin (immobilised with antibody)	(0/583+35/473+0/468)+ (1/502+2/460+26/450+3/500+5/500)	(8/583+13/473+8/468)+ (0/502+0/460+0/450+0/500+0/500)	(11/583+18/473+29/468)+ (31/502+16/460+29/450+25/500+38/ 500)	
	1.8%	1.7%	5.0%	8.5
RGD Blocked Integrin	(65/500+61/500+86/500)+(50/501+73/ 500+34/416+27/410+52/320)	(8/500+0/500+4/500) + (0/501+0/500+0/416+0/410+0/320)	(18/500+22/500+12/500)+ (3/501+3/500+5/416+13/410+0/320)	
	12.3%	0.8%	5.1%	18.2
Antibody	(0/1000)+(4/330+19/501+17/320+50/5 01+18/500	(65/1000)+(0/330+0/501+22/320+4/5 01+13/500)	(36/500+26/500)+(7/330+36/501+4/ 320+11/501+0/500)	
	5.1	3.0	3.8	11.9
Silane	204/989	(37/489+13/500)	(2/489+3/500)	
	20.6%	5.1%	0.5%	25.7

*(number of curves with interaction/ total number of curves) of the first measurement + (number of curves with interaction/ total number of curves) of the second measurement

Appendix H. Base of frequency count for Figure 5.16

A-Table 6. Count of jumps for Figure 5.16

Surface	Peeling*	Large Force Jump*	Sum
Silane	204/989	(37/489+13/500)	
	20.6 %	5.1 %	25.7%
Silane with MQ-water	(4/500+5/500)	(496/500+495/500)	
	0.9 %	99.1 %	100%

*(number of curves with interaction/ total number of curves)